AD-A116 284 UNITED STATES STEEL CORP MONROEVILLE PA RESEARCH LAB F/G 19/6
CHARACTERIZATION OF 'WHITE LAYER' AND CHROME PLATING ON FIRED C--ETC(U)
JUN 82 R M FISHER, A SZIRMAE DAAA22-81-C-0121

UNCLASSIFIED ARLCB-CR-82014 NL

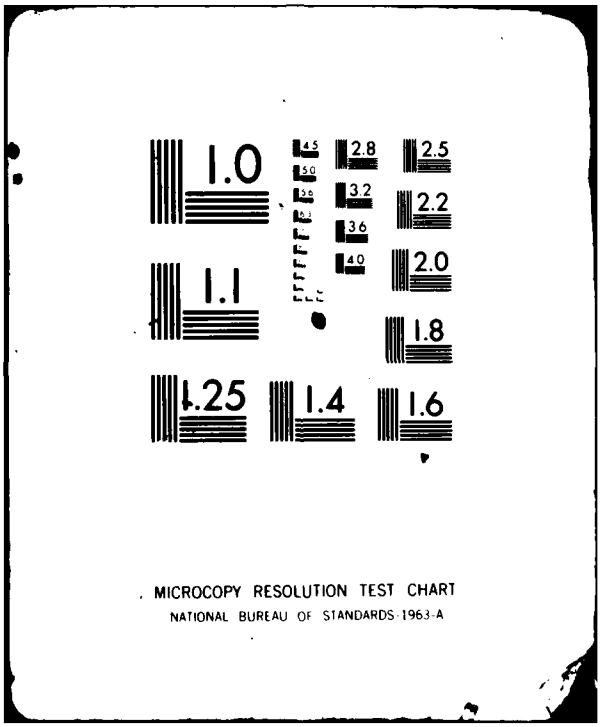
1.0
1.1
1.25
1.4
1.6
1.8
2.0
2.2
2.5
2.8
3.2
3.6
4.0
4.5
5.0
MICROCOPY RESOLUTION TEST CHART
NATIONAL BUREAU OF STANDARDS-1963-A

CONTRACTOR REPORT ARLCB-CR-82014

CHARACTERIZATION OF "WHITE LAYER" AND CHROME PLATING ON FIRED CANNON AND ON LABORATORY SIMULATION SAMPLES

R. M. Fisher and A. Szirmae
U. S. Steel Corp., Research Laboratory
Monroeville, Pa. 15146

June 1982

US ARMY ARMAMENT RESEARCH AND DEVELOPMENT COMMAND
LARGE CALIBER WEAPON SYSTEMS LABORATORY
BENÉT WEAPONS LABORATORY
WATERVLIET, N. Y. 12189

Dr. M. H. Kamdar
Research Engineer
Benet Weapons Laboratory
ARRADCOM

DISCLAIMER

The findings in this report are not to be construed as an official Department of the Army position unless so designated by other authorized documents.

The use of trade name(s) and/or manufacture(s) does not constitute an official indorsement or approval.

DISPOSITION

Destroy this report when it is no longer needed. Do not return it to the originator.

SECURITY CLASSIFICATION OF THIS PAGE *(When Data Entered)*

REPORT DOCUMENTATION PAGE	READ INSTRUCTIONS BEFORE COMPLETING FORM
1. REPORT NUMBER: Contractor Report ARLCB-CR-82014	2. GOVT ACCESSION NO.: AD-A116 284
	3. RECIPIENT'S CATALOG NUMBER:
4. TITLE *(and Subtitle)*: CHARACTERIZATION OF "WHITE LAYER" AND CHROME PLATING ON FIRED CANNON AND ON LABORATORY SIMULATION SAMPLES	5. TYPE OF REPORT & PERIOD COVERED: Final, Jan. 1981 - Jan. 1982
	6. PERFORMING ORG. REPORT NUMBER:
7. AUTHOR(s): R. M. Fisher and A. Szirmae, United States Steel Corporation; Dr. M. H. Kamdar, Research Engineer, ARRADCOM	8. CONTRACT OR GRANT NUMBER(s): DAAA22-81-C-0121
9. PERFORMING ORGANIZATION NAME AND ADDRESS: United States Steel Corporation, Research Laboratory, Monroeville, PA 15146	10. PROGRAM ELEMENT, PROJECT, TASK AREA & WORK UNIT NUMBERS:
11. CONTROLLING OFFICE NAME AND ADDRESS: US Army Armament Research & Development Command, Large Caliber Weapon Systems Laboratory, Dover, NJ 07801	12. REPORT DATE: June 1982
	13. NUMBER OF PAGES: 55
14. MONITORING AGENCY NAME & ADDRESS *(if different from Controlling Office)*: US Army Armament Research & Development Command, Benet Weapons Laboratory, DRDAR-LCB-RM, Watervliet, NY 12189	15. SECURITY CLASS. *(of this report)*: UNCLASSIFIED
	15a. DECLASSIFICATION/DOWNGRADING SCHEDULE:
16. DISTRIBUTION STATEMENT *(of this Report)*: Approved for public release; distribution unlimited.	
17. DISTRIBUTION STATEMENT *(of the abstract entered in Block 20, if different from Report)*:	
18. SUPPLEMENTARY NOTES:	
19. KEY WORDS *(Continue on reverse side if necessary and identify by block number)*: Weapons, Artillery--Guns, Stresses, White Layer, Chromium, Plating, Iron Carbide, Alloy Steels, Alloy Steels--4000 Series, Chemical Composition, Cracking-Failure, Surface Properties, Microstructure, Grain Structure, 4340 Steel, Simulation, Ordnance, Austenite, Cementite.	

20. ABSTRACT *(Continue on reverse side if necessary and identify by block number)*

This work confirms that the effect of exposure of 4340 steel cannon tubes to firing is the formation of Fe_3C and 1% C-austenite on the surface. The stress generated by the explosion results in the formation of rather uniform networks of shallow and deep cracks. Particular attention was given to the structure of these cracks because they contained TiO_2 (sometimes added to the charge), Cu, S, and Al. Examination of the microstructure of electrodeposited

(CONT'D ON REVERSE)

DD FORM 1 JAN 73 1473 EDITION OF 1 NOV 65 IS OBSOLETE

UNCLASSIFIED

SECURITY CLASSIFICATION OF THIS PAGE *(When Data Entered)*

20. ABSTRACT (CONT'D)

chromium revealed a strong dependence of grain structure on plating conditions. The void space between the aligned cylindrical grains is probably responsible for the high tensile stresses in chrome plating and the propensity for severe cracking.

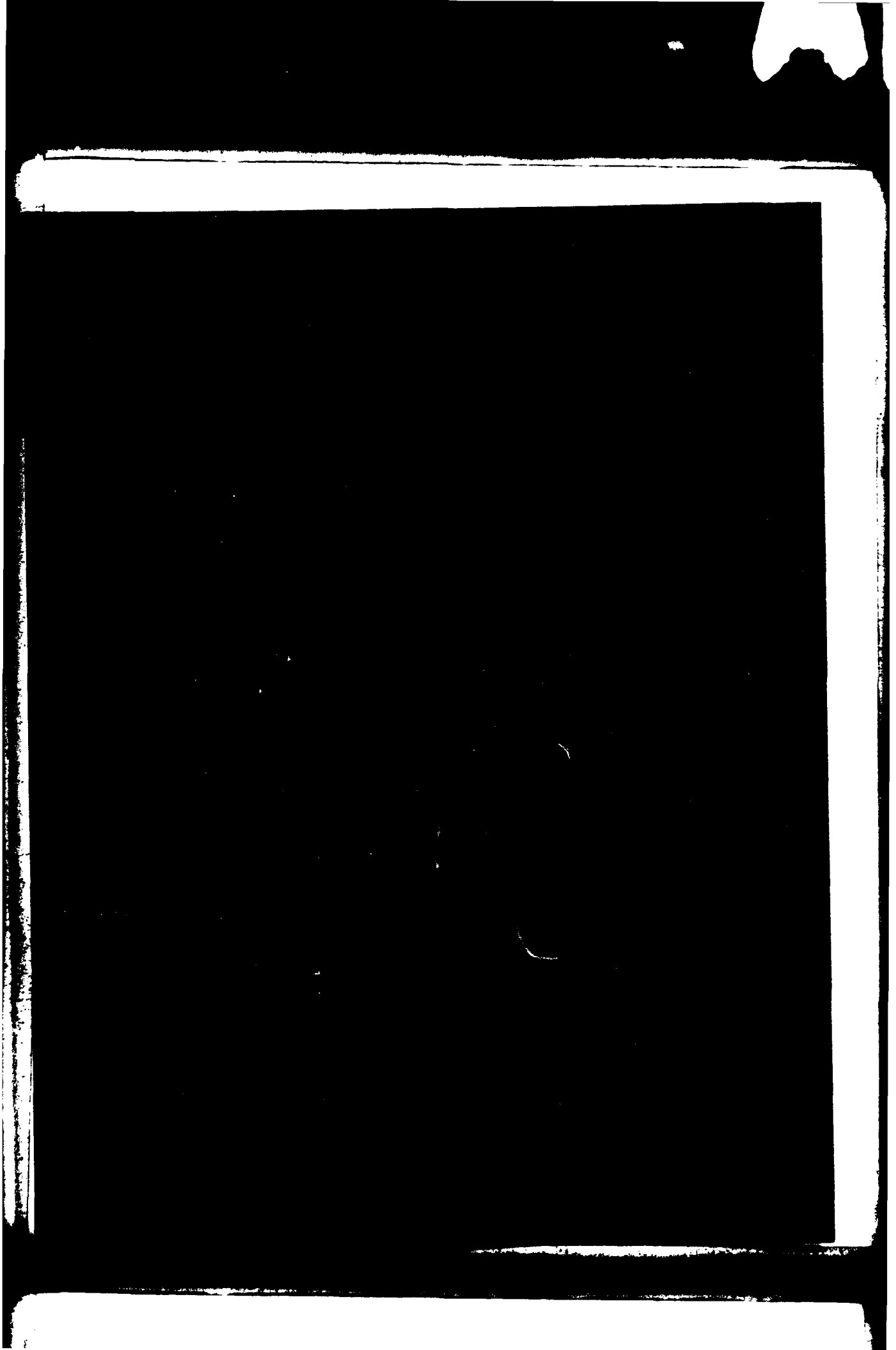

PART ONE

CHARACTERIZATION OF "WHITE LAYER" AND CHROME PLATING ON FIRED CANNON AND ON LABORATORY SIMULATION SAMPLES

SUMMARY

Introduction

The nature of the surface alterations that occur on the bore surface of cannon tubes during firing has been the subject of considerable research for many years at Watervliet Arsenal[1] and elsewhere.[2] The successful development of equipment to form "white layer" (etch-resistant composite of cementite and high-carbon austenite) in the laboratory by pulse heating in high-pressure methane has facilitated systematic investigation.[3] Previous studies at this Laboratory[4] of both fired cannon and laboratory simulation samples revealed that the high temperature and high-pressure gas generated during firing can cause intense carburization of the steel surface. Various experimental techniques, including high-voltage and scanning electron microscopy, Mossbauer, Auger, and secondary-ion mass spectroscopy were used to characterize the affected surfaces. These experimental techniques are illustrated schematically in Figure 1a, and the results of the previous study are illustrated in Figure 1b.

As shown in Figure 1, crystals of Fe_3C and solidified iron carbon eutectic form on the outer surface. High carbon austenite occurs to a depth of 10-20 um, along with some martensite transformation. The boundary between the austenite and the steel matrix, sometimes called "altered ferrite," was found to consist of intermediate carbon martensite characteristic of a very fine grain austenite parent phase. This region represents the maximum penetration of the heat-affected zone where ferrite to austenite to martensite cycling occurs during heating

and cooling.

The purpose of this present investigation was to extend the study by examining additional specimens and refining the analytical procedures. All the various experimental observations are recorded in this report. The results of some phases of the work are suitable for publication in the metallurgical literature, and drafts of several papers describing and interpreting the present and previous studies will be prepared in due course.

Experimental Methods

Representative samples of 4340 steel, cut from actual fired cannons, as well as materials used in laboratory simulation studies, were provided by Dr. M. Kamdar of Watervliet Arsenal. Their specific identification and description are listed below.

"White Layer" Samples

Code	Description
T-45	Fired-Cannon Tube - 4340 Steel
N-11	Pulse-Heated in Methane - 3000 psi

Characterization of the surface structure utilized most of the techniques in the first phase of this study. As before, Mossbauer analysis (Table I) of the surfaces of the samples was carried out before they were cut or otherwise prepared for metallographic examination. However, Auger analysis and secondary ion mass spectroscopy studies were not conducted. Instead, considerable emphasis was put on examining the deeply penetrating cracks that result during firing because of the significance of previously unnoted features. Ion thinning was used successfully to prepare a thin foil at the carbide-austenite interface on a labora-

tory simulation sample.

Results and Discussion

Scanning electron micrographs of the bore surface of fired cannon T-45 are shown in Figure 2, along with the X-ray spectra of one of the hillocks. The characteristic craze pattern of the hillocks was observed previously; however, the presence of a large quantity of titanium in the X-ray signal was a surprise. This observation led to more detailed investigation of the titanium-covered surface. Other examples of scanning electron micrographs of the bore surface after ultrasonic cleaning and light mechanical polishing to remove the debris are shown in Figure 3. Note that both an overall scan such as shown in 3a and point analysis on a single hillock in 3b show a very high level of titanium. The iron intensity comes from regions where the steel is not covered by the Ti coating.

A sample that was more heavily ground and polished is shown in Figure 4. The depth of grind increases from the lower right corner to the upper left in the top micrograph. The X-ray analysis shows a very low level of titanium but a substantial quantity of aluminum and copper. In this area, the sample was ground to below the white layer so that the bare metal surface was exposed.

Scanning electron micrographs, taken at a point in the sample where the depth of grind was even greater, are illustrated in Figure 5. Both regions show a very high level of aluminum and copper, and region (d) reveals the presence of a considerable amount of sulfur as well. The next series of micrographs shown in Figure 6 are even further along the taper section where the depth of grind is considerable; even here, perhaps 200 microns below the surface, the aluminum and copper levels are surprisingly high in the crack. These elements were found right up to the tip of the crack, as illustrated in the micrographs and X-ray

spectra shown in Figure 7. In some regions there is a very high sulfur level, as for example point (d), and even at (e) where the crack is extremely narrow (very near to the tip) the occurrence of copper, aluminum, and sulfur is clearly evident. The importance of these elements and their possible origin will be discussed in the following section of this report.

Scanning electron micrographs of a 16° taper cross section of a nickel-plated sample of cannon tube T-45 are shown in Figure 8. Again, it may be noted that aluminum, titanium and copper are present in the cracks, along with some nickel that apparently penetrated during the plating process. Note the dual crack structure comprising a series of very shallow closely spaced cracks shown in the left of micrograph 8b, and a network of cracks with much larger spacing in the central area. Optical and scanning electron micrographs of the etched 16° taper cross section of cannon tube (T-45) are shown in Figure 9. These micrographs illustrate the essential features that result from white-layer formation. Starting at the top (in the steel matrix) and proceeding toward the surface, the first region is the "altered ferrite" region, which is the heat-affected zone where the steel is cycled through the austenite-martensite transformation. Because of the high alloy content, this steel has considerable hardenability and the slow cooling rate due to the self-quenching in the steel tube is still sufficient for some martensite to form. The lighter etched area is altered austenite, which contains a large amount of substructure. Finally, the lower optical micrograph in Figure 9b shows an outer thin white rim over the surface.

The constituents in the microstructure are somewhat more evident in the scanning electron micrograph in Figure 9. Again proceeding from top to bottom, the first area corresponds to the altered austenite structure, then a narrow rim of white etch-resistant austenite. The next layer is a titanium phase which we will discuss later and, finally, the very bottom of the micrograph shows the smooth outer rim of nickel plating that was applied to

protect the surface during polishing.

Optical and scanning micrographs at higher magnification in Figure 10 show the white etch-resistant rim of high carbon austenite. The x-ray spectra of the regions marked show the penetration of the nickel plating, the occurrence of titanium, sulfur, copper, aluminum, and some other elements at lower concentrations in both areas. Optical and electron scanning micrographs of another point on the surface of the polished and etched 16° taper cross section of tube T-45 are shown in Figure 11. Of particular interest here is the white etch-resistant material well in below the surface, that is, in the "altered ferrite" region. As shown in the X-ray spectra, this region is generally very high in copper, with some nickel penetration during plating evident along with a fairly large amount of sulfur in some regions. The composition varied along these crack penetration zones; a number of them were analyzed and the results shown here are quite typical.

Very low angle (3°) taper cross sections of nickel-plated samples were also prepared, as illustrated in Figure 12. The optical micrograph (b) in Figure 12 shows the titanium-rich layer on the surface of some hillocks, the white austenite rim magnified in width because of the taper section, and the etched altered ferrite area. Microhardness testing at Watervliet provided the data illustrated in Figure 12d, which demonstrates that the hardness of the etch-resistant austenite rim is relatively low compared with the very high values for the altered austenite and altered ferrite regions.

Attempts to use Auger spectroscopy to determine the carbon content of the austenite were not totally successful. Small- area Auger scans in the ferrite and in the austenite regions are shown in Figure 13. Comparison of the carbon peaks suggests that the carbon level in the austenite is about three t' as higher than that in the ferrite; that is, about 1.2 wt %.

This value is in keeping with the results of analysis by other techniques as reported in the first report.[4]

Attempts to obtain a quantitative profile by Auger analysis were not successful. The individual points are shown as marked with a white spot next to the dark reference mark in Figure 14a. The values scattered somewhat, probably due to surface roughness, so that a carbon profile could not be determined. The lower half of the figure shows two scanning Auger micrographs taken of the same area as Figure 14a, using oxygen and titanium, indicating that the titanium region on the surface is actually titanium oxide. The little white square patch in the oxygen image is the result of electron-induced oxidation from residual gases in the Auger microprobe. The penetration of titanium well up into the cracks is quite evident in these scanning images.

Cracks in the fired cannon tube were examined in both the longitudinal and transverse cross sections. The transverse cross sections are useful for illustrating the extreme depth of penetration of some of the cracks, as illustrated in Figure 15. These depths are well beyond the point where copper was observed. Specific measurements of the maximum depth of copper penetration were not obtained.

Results of this more recent study are illustrated schematically in Figure 16. It may be noted that the outer surface consists of a fairly thin region of TiO_2 covering the hillocks and penetrating well into the cracks. The presence of copper, aluminum, and sulfur within the cracks is also shown in the figure. This may result from the use of copper on the rotating bands, as copper was found on the surface of test plugs used and described in the report by Griffen et al.[1] The origin of the sulfur is not clear at this point, nor is the source of the aluminum. Since alumina was used for polishing, it is possible that some of the aluminum observed was the result of small particles of polishing abrasive that had been trapped in the various

cracks. Certainly the aluminum content did vary from point to point. On the other hand, careful inspection of several cracks indicated that the aluminum was quite uniformly distributed in local regions.

Laboratory Simulation Samples

The results from the previous study of surface alterations during laboratory simulation testing are shown schematically in Figure 17. The various metallographic techniques reveal that a surface film of iron-carbon eutectic overlayed a high-carbon austenite region, some plate martensite, and an altered

Optical and scanning electron micrographs of a low-angle taper section of the surface of laboratory simulation sample N-11 are shown in Figures 18 and 19. The characteristic eutectic structure seen earlier is very evident, and it may be noted that the tips of some of the carbides project into the metal (since this is a low-angle taper section, the lower half of the micrographs show the subsurface). A puzzling feature of the micrograph in Figure 18 is that etching causes some regions of the eutectic to appear white in the optical micrograph, and appear dark in the scanning electron micrograph. At the moment we have no explanation for the origin of these contrasting effects.

The scanning electron micrograph of the carbide-austenite interface in Figure 20a also shows a f ew of the pools of austenite with evidence of martensite transformation. These pools were much more numerous in other simulation samples. Thin foils of the carbide-austenite interface were prepared successfully by grinding and ion thinning, as shown in Figure 20b. The iron-carbide eutectic appears in the upper half of the micrograph and the underlying austenite area in the lower half. Other transmission electron micrographs of the carbide-austenite interface are shown in Figure 21. Because of bending, the diffraction contrast from both the carbide and austenite regions in the thin foil varies considerably. The occurence of annealing twins and dis-

locations is illustrated in Figure 21c. The austenite also exhibits several as yet uninterpreted microstructural features. The micrograph in Figure 21b shows a group of lenticular areas containing fine striations which are reminiscent of but not identical to martensite plates. Other austenite areas, shown in the lower halves of Figures 21a and 22a, also exhibit very fine striations. In both cases these structures may result from precipitation of fine carbides on faults resulting from plastic deformation during rapid cooling. High resolution electron microscopy will be required to identify the specific nature of this structure, which is presumably responsible for the high hardness. The martensitic structure in the altered ferrite region is illustrated in Figure 22b.

In summary, the microstructure of white layer in the new laboratory simulation samples is very similar to that seen previously, and is illustrated schematically in Figure 17.

Conclusions

The new finding in this study is that cannon tubes that were fired using an explosive which contained titanium powder are coated with TiO_2; this material penetrates part way into the cracks. However, the more important feature of the cracks is the presence of a rather high concentration of copper, sulfur, and aluminum. The copper would cause an unusual form of hot-shortness and cracking of the steel base as a result of the high mechanical and thermal stresses generated during firing.

The origin of the periodic craze structure is still not clear. The heat pulse would result in about a 1 to 2 percent thermal expansion and contraction at the surface. High-temperature deformation during the heating cycle could accommodate the compressive stresses during expansion; however, as cooling occurred, deformation might be more restricted. Thus, high tensile stresses developed in the outer layers could lead to crack

penetration, as observed by metallographic techniques. The coarse spacing and deep penetrating cracks are rotated perhaps 15 degrees to the tube axis - about the same angle as the rifling. This may result from coupling of a torsion stress through the rifling as the projectile is accelerated, giving the barrel a slight twist causing the crack pattern that is observed.

References

1. R. B. Griffin, J. Pepe and C. Morris, "Metallurgical Examination of Bore Surface Damage in a 5-inch Gun," Metallography 8, 1975, pp. 453-71.

2. J. D. Venables, "Characterization of Bore Surfaces on Large Gun Barrels," Martin-Marietta Report to Watervliet Arsenal MML-TR-76-55C, July 1976.

3. M. K. Kamdar, A. Campbell and T. Brassard, "A Metallographic Study of White Layer in Gun Steel," ARRADCOM Report ARLCB-TR-78012, August 1978.

4. R. M. Fisher and A. Szirmae, "Characterization of 'White Layer' Formation on a Fired Cannon and on Laboratory Simulation Samples," U. S. Steel Research Report to Watervliet Arsenal, Contract DAAA22-81-C0121, March 1981.

TABLE I

SUMMARY OF MOSSBAUER ANALYSIS

Sample	Composition*
Tube 6826	14% austenite
	35% ferrite
	28% cementite
	22% unknown (rust?-carbide?)
Tube 45	33% austenite (5.8 atomic %C)
	60% ferrite
	7% cementite
Laboratory Simulation	38% austenite (3.7 atomic %C)
	55% ferrite
	7% cementite

*outer 2-3 μm.

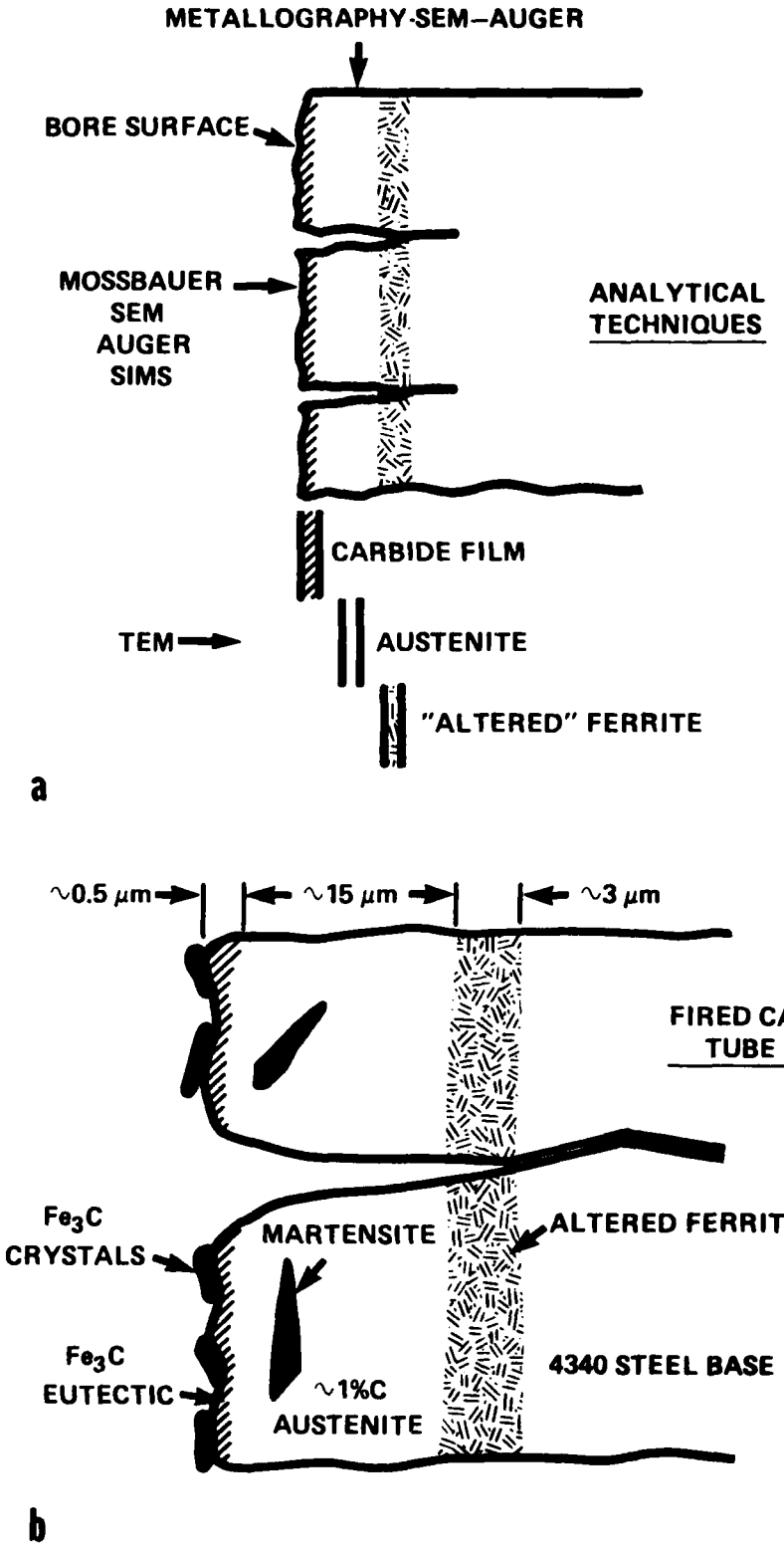

Fig. 1. Schematic illustration of analytical techniques utilized to characterize the bore surfaces of fired cannons (a), and summary of results of previous investigation (b).

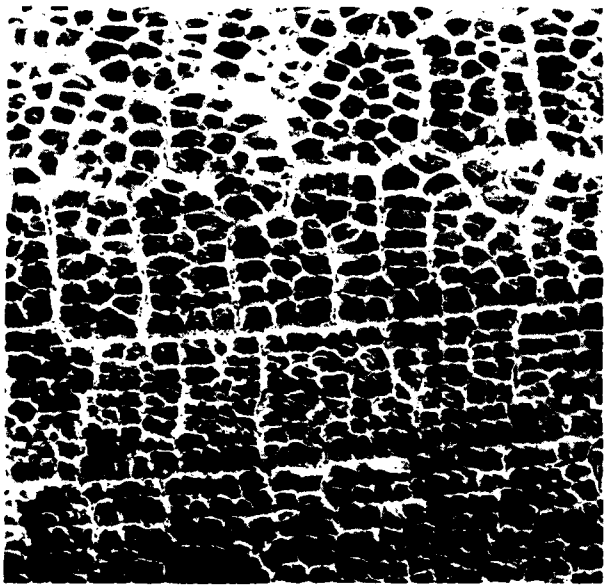

(a) 20X

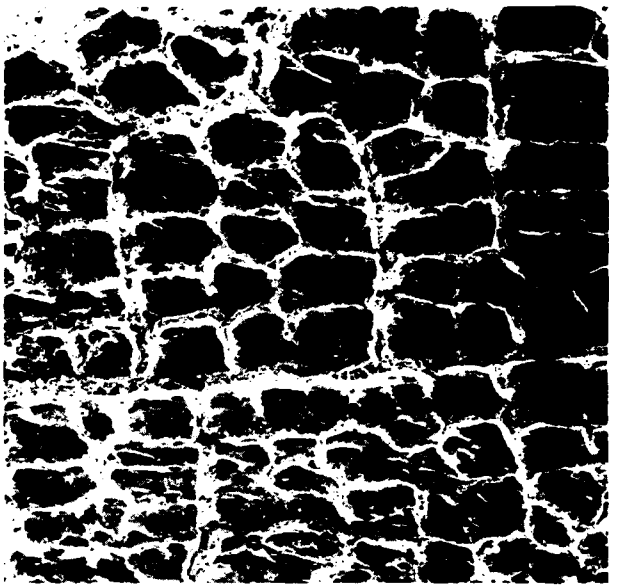

(b) 50X

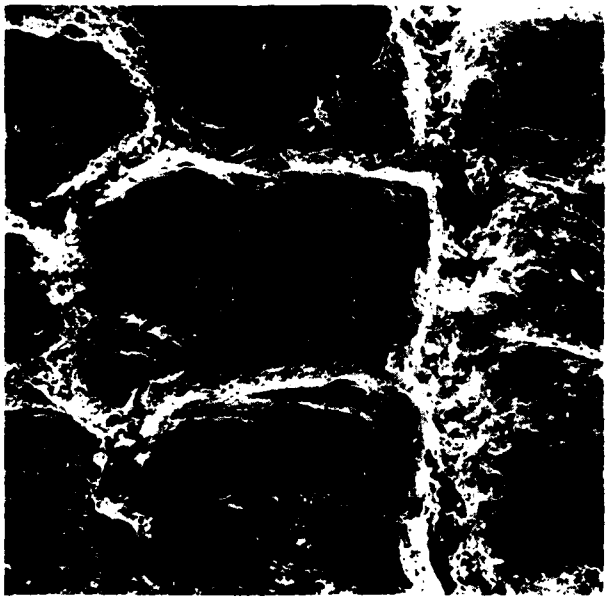

(c) 200X

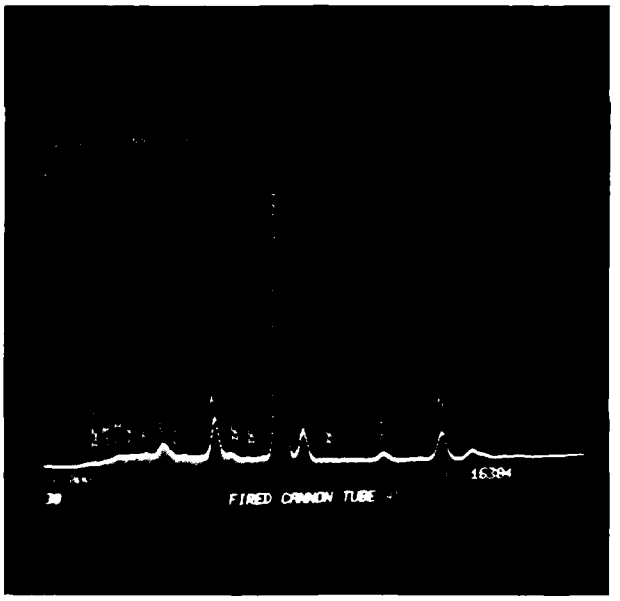

(d)

Scanning electron micrographs of as-received bore surface of cannon tube (T-45) illustrating characteristic craze pattern (a,b,c,), and X-ray spectra (d) from the central area in (c).

Figure 2

(a) 60X

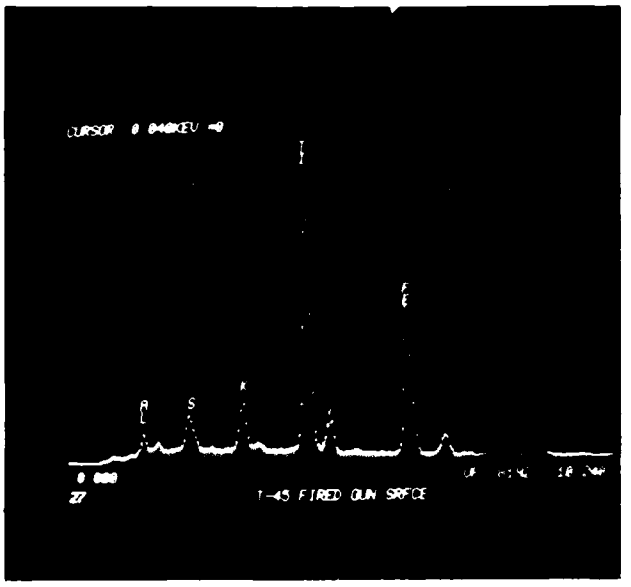

(b)

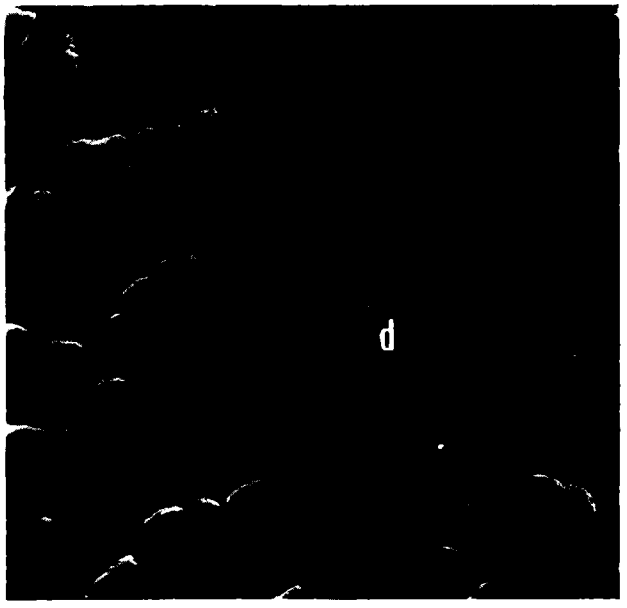

(c) 120X

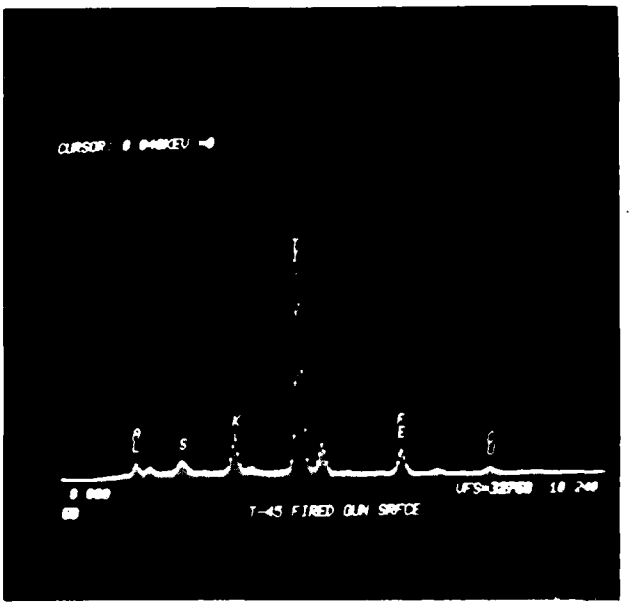

(d)

Scanning electron micrographs of bore surface after light polishing and cleaning. X-ray spectra in (b) from area shown in (a) and in (d) from single point as marked.

Figure 3

20X

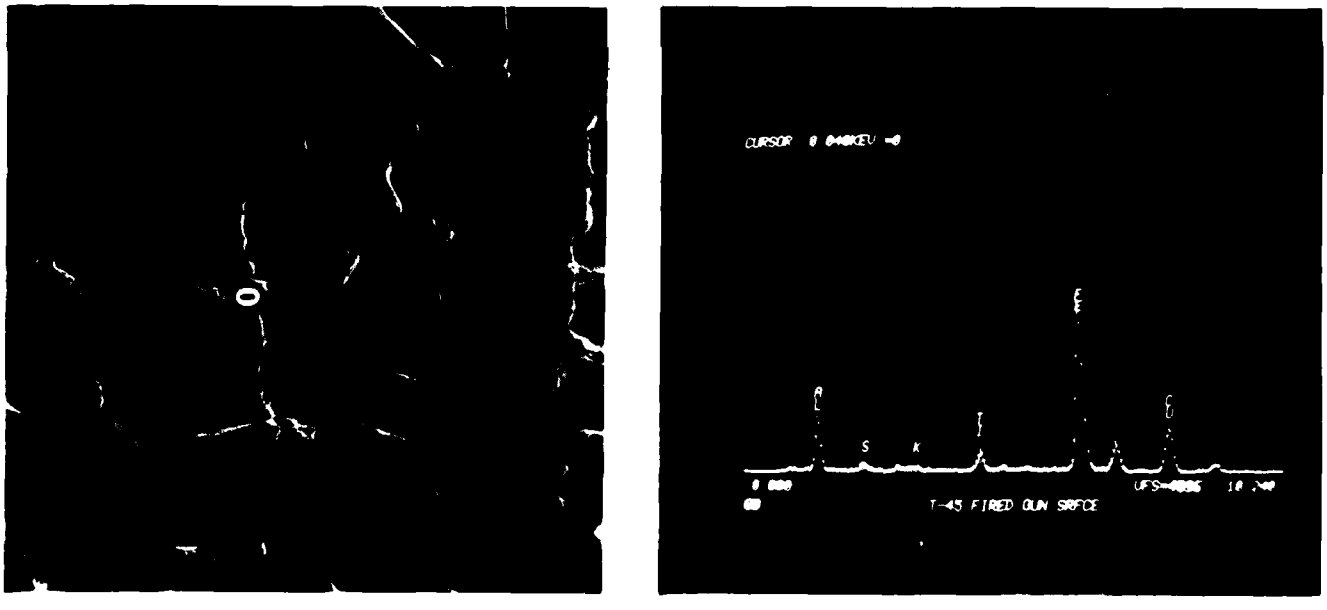

120X

Bore surface after grinding and polishing to remove outer layer; depth of polishing increases from lower right to upper left.

Figure 4

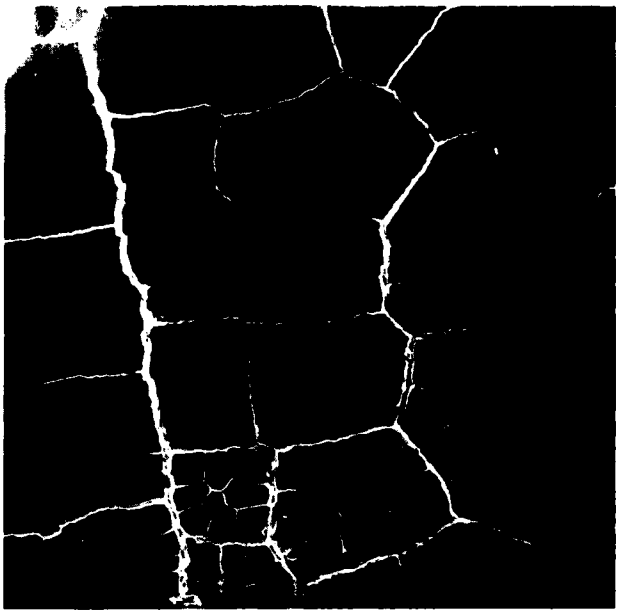

(a) 30X

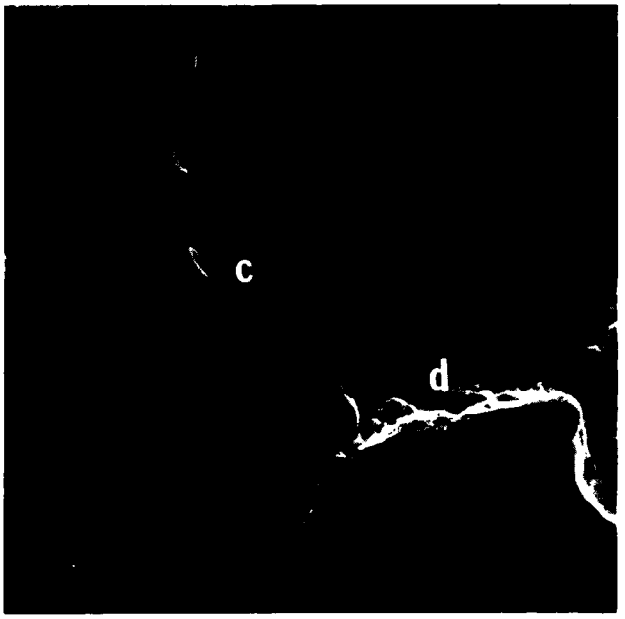

(b) 600X

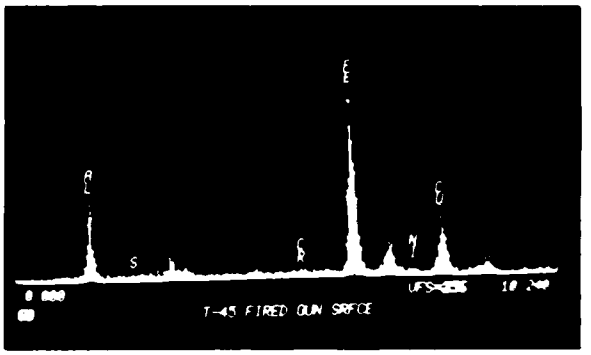

(c)

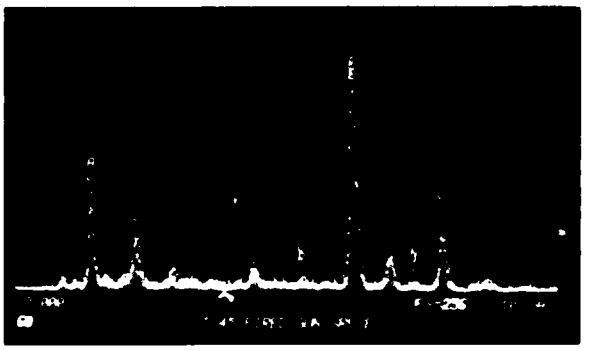

(d)

Scanning electron micrographs and X-ray spectra of material in cracks near to the surface.

Figure 5

60X

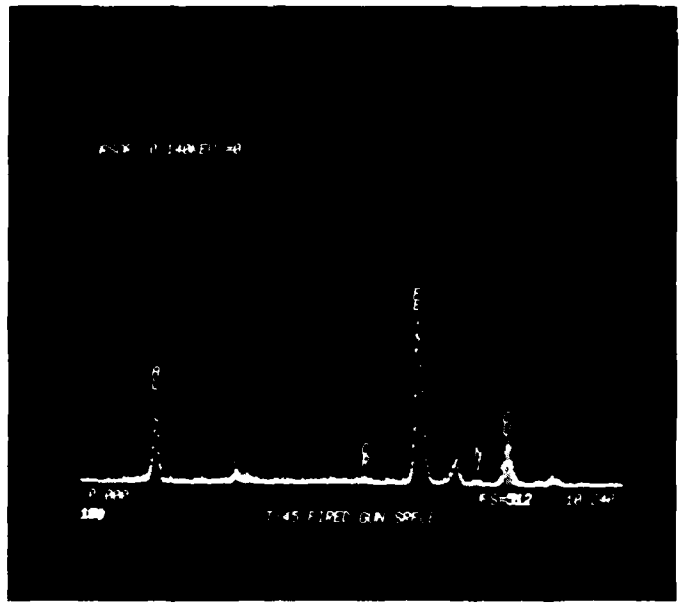

600X

Scanning micrographs and X-ray spectra of material in cracks about 200 μm below the surface.

Figure 6

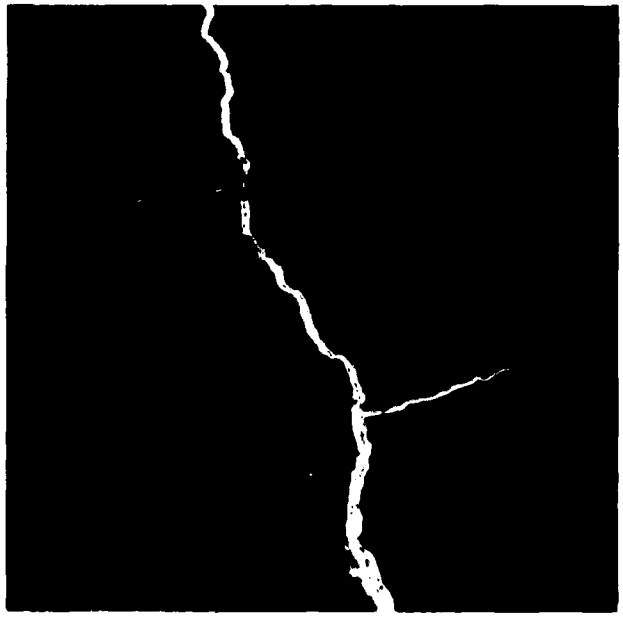

(a) 60X

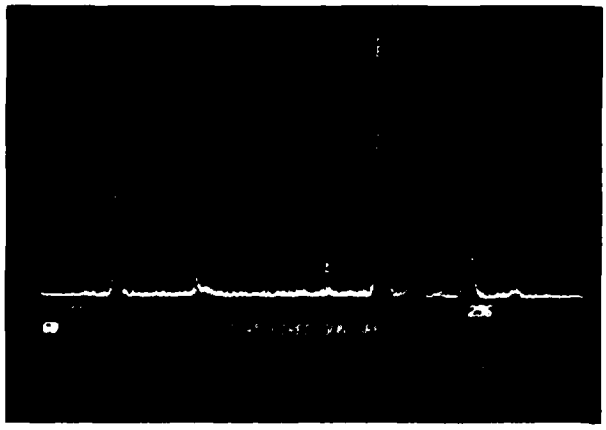

(b)

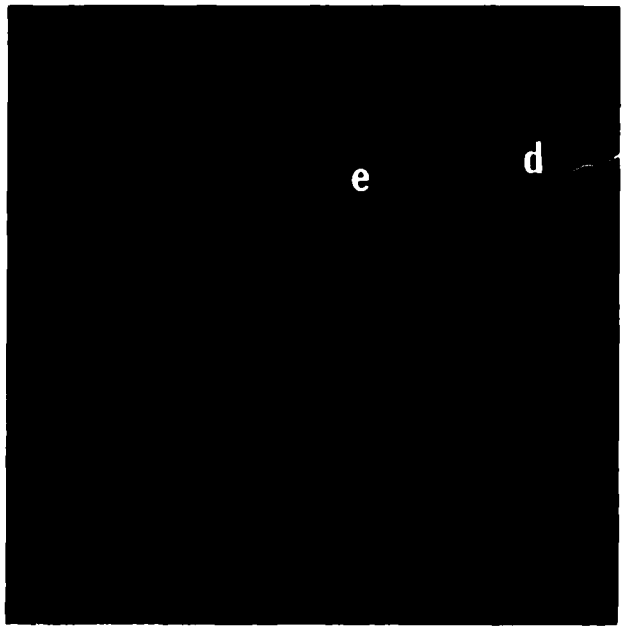

(c) 300X

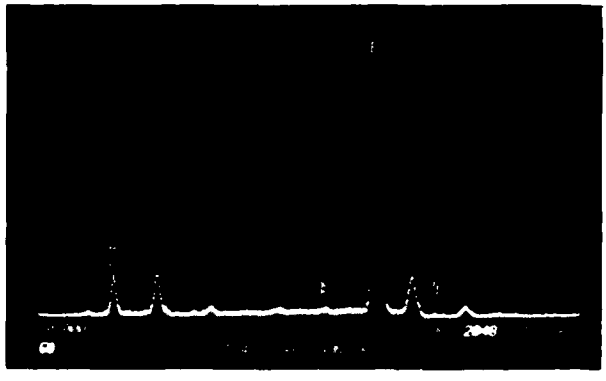

(d)

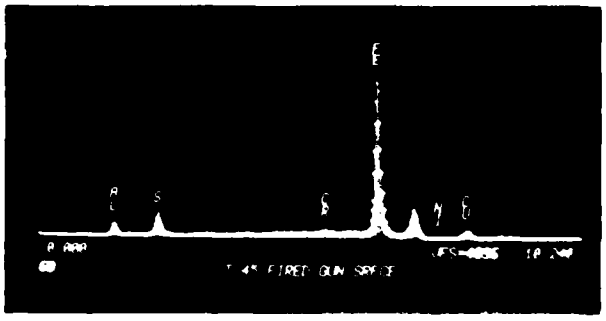

(e)

Scanning micrographs and X-ray spectra of material near to the tips of cracks.

Figure 7

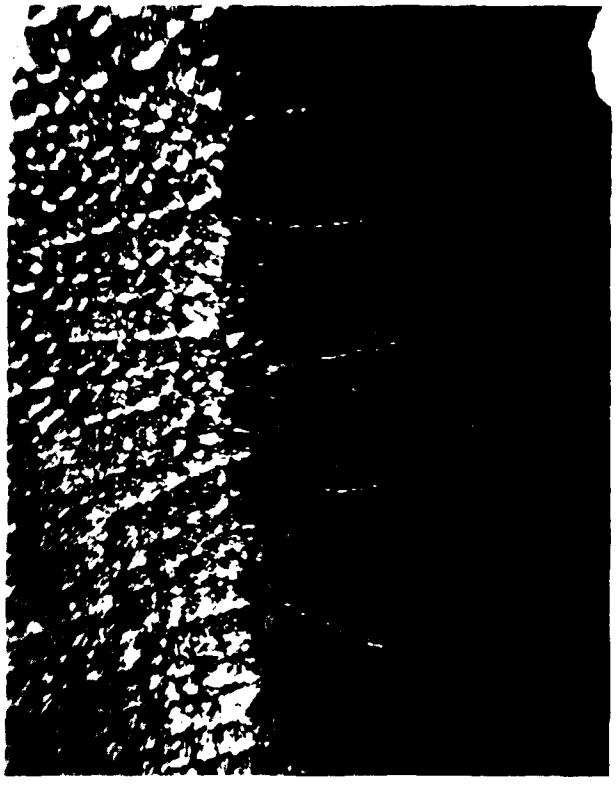

(a) 30X

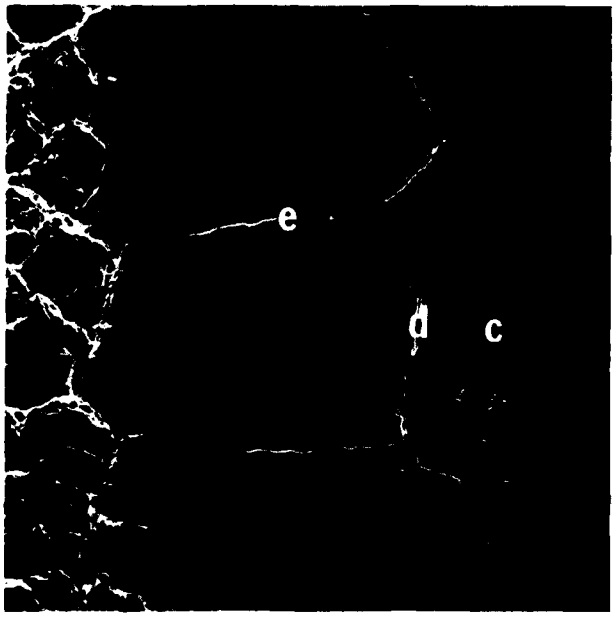

(b) 50X

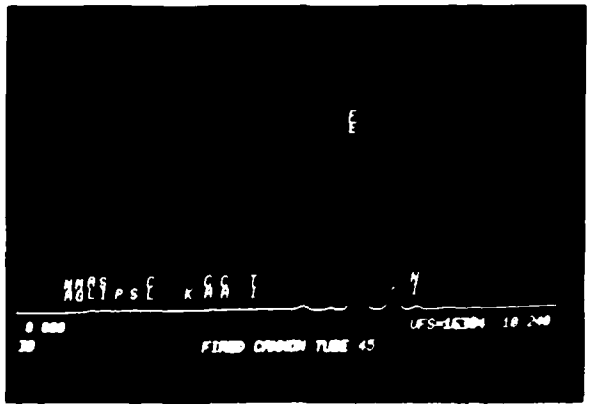

(c)

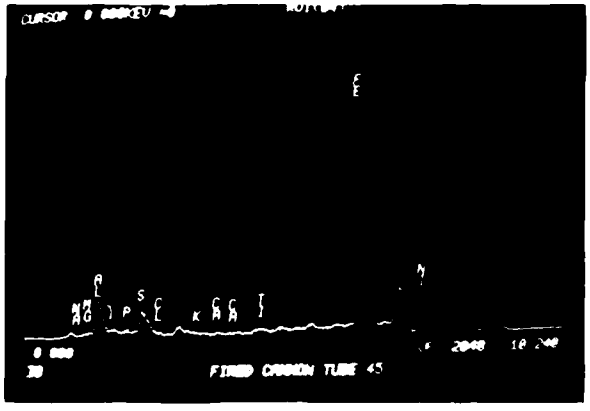

(d)

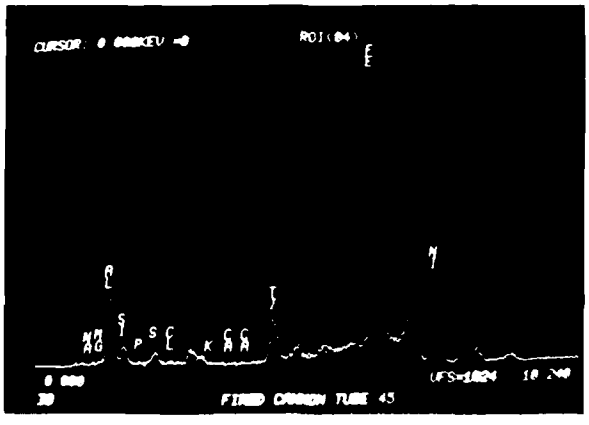

(e)

Scanning micrographs of a 16° taper section of a Ni-plated sample of cannon tube (T-45). Al and Cu are detected well into the crack along with evidence of penetration of Ni during plating.

Figure 8

(a) 100X

(b) 200X

(c) 300X

Optical and scanning micrographs of etched 16° taper cross section of cannon tube (T-45).

Figure 9

(a) 500X

(b) 500X

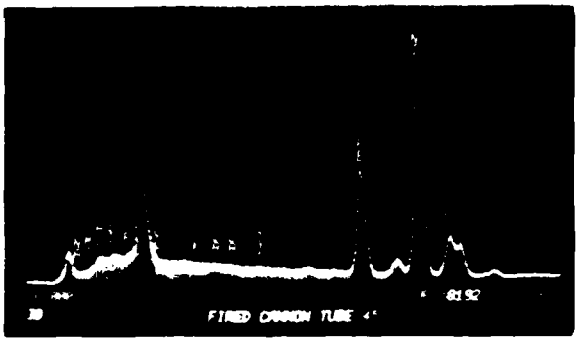

(c)

(d)

Optical and scanning micrographs of etched 16° taper cross section of cannon tube (T-45).

Figure 10

(a) 500X

(b) 200X

(c) 1200X

(d)

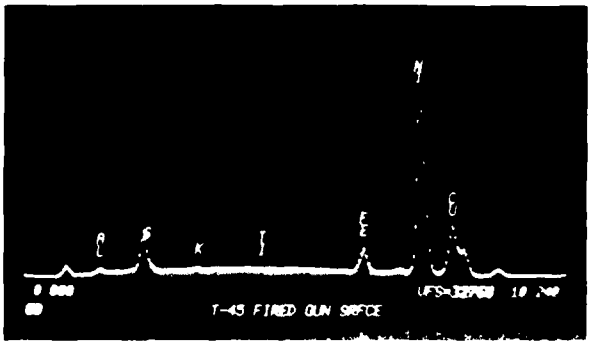

(e)

Optical and scanning micrographs of etched 16° taper cross section of cannon tube (T-45).

Figure 11

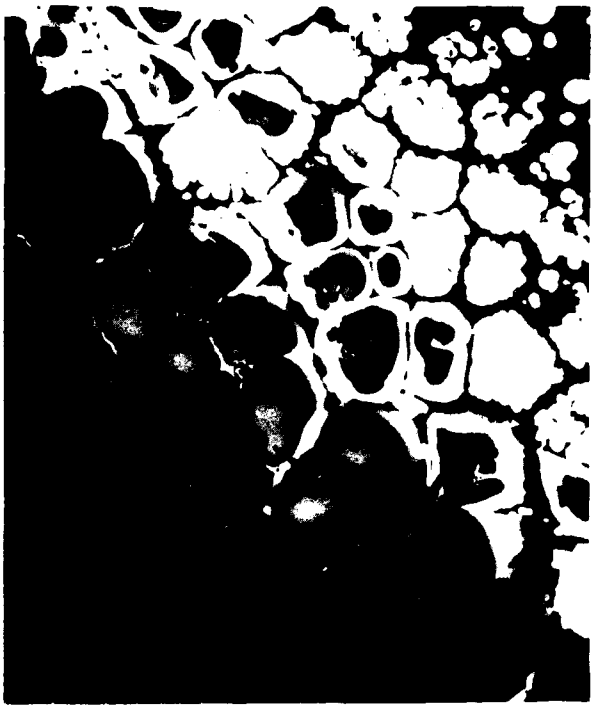

(a) 50X

(b) 150X

(c) 500X

(d) 1000X

Optical and scanning electron micrograph[illegible]f 3° Ni-plated cross section of T-45. White areas are [illegible]ckel plating. Areas marked in (c) were analyzed for carbon by Auger spectroscopy.

Figure 12

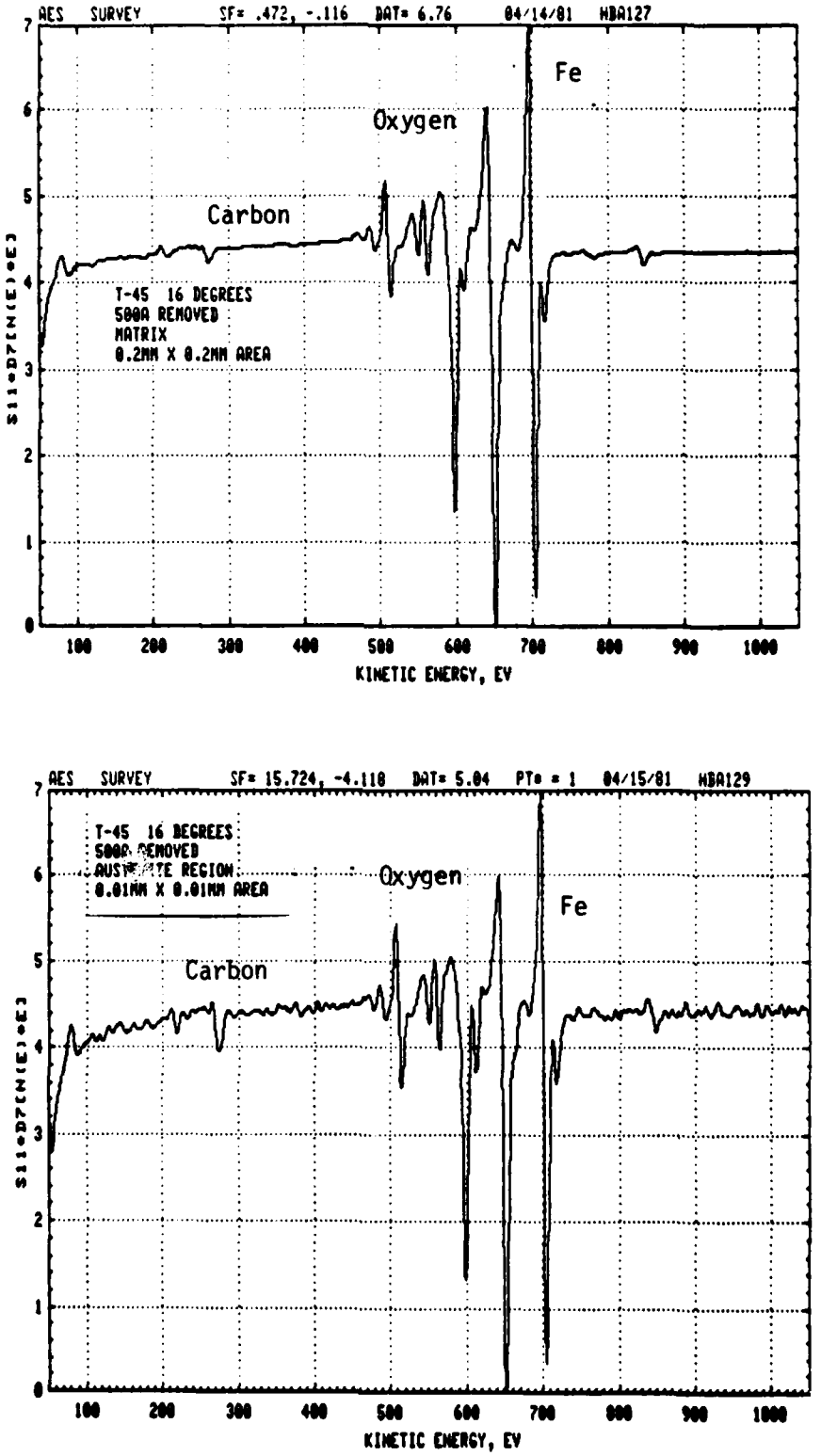

Fig. 13. Auger spectra of steel matrix (top) and subsurface austenite (bottom - see figure 14).

(a) 400X

(b) 400X

(c) 400X

Scanning electron micrograph of areas of taper section of tube (T-45) analyzed by Auger spectroscopy (top), and oxygen and titanium scanning Auger images of surface material.

Figure 14

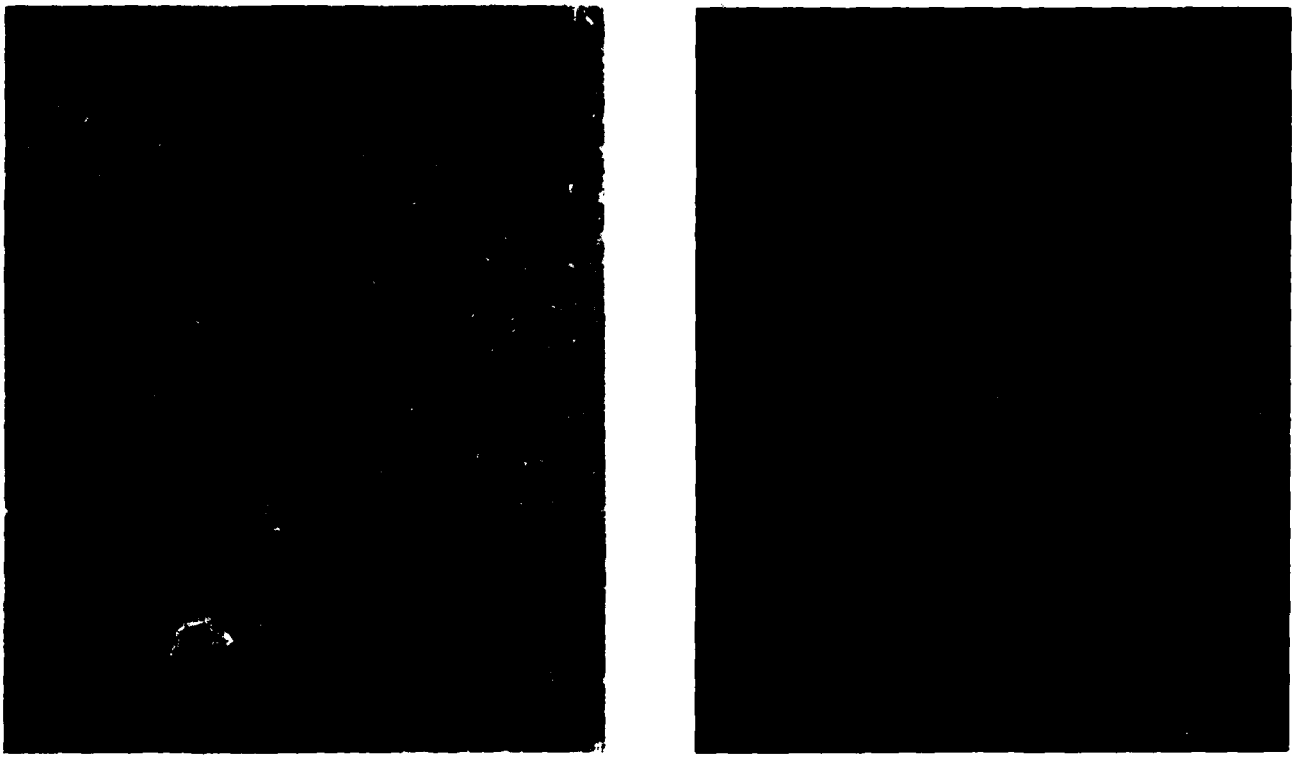

(a) 200X (b) 1000X

Optical micrographs of typical cracks as seen in end view cross section of tube (T-45).

Figure 15

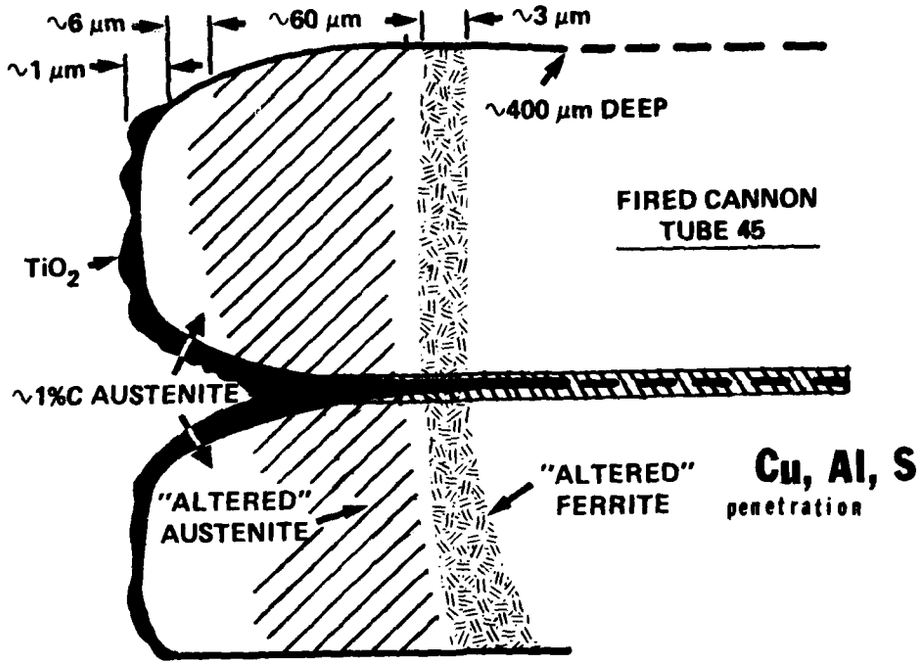

Fig. 16. Schematic illustration of surface structure of cannon tube.

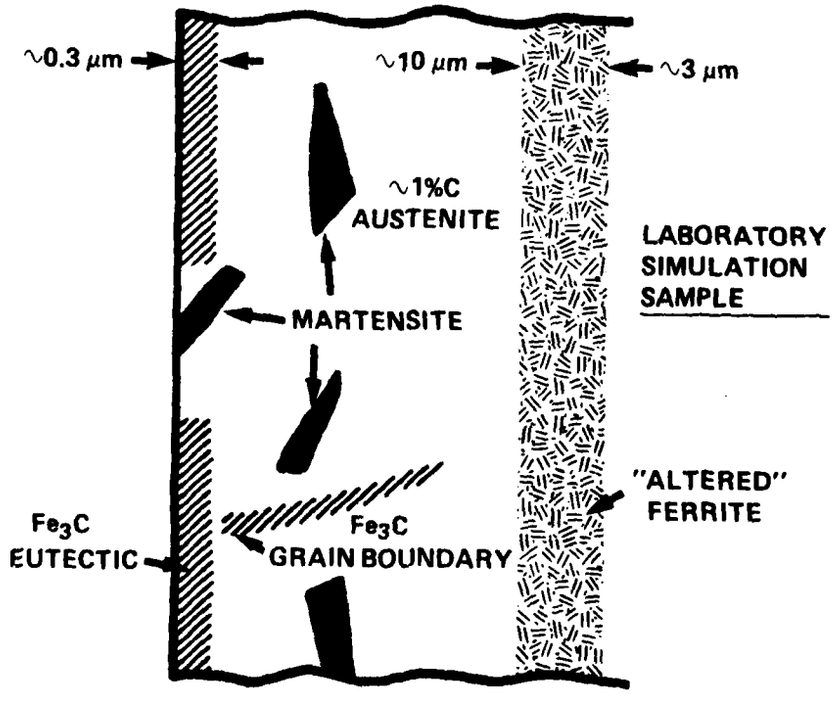

Fig. 17. Schematic illustration of previous observations of surface region of laboratory sample.

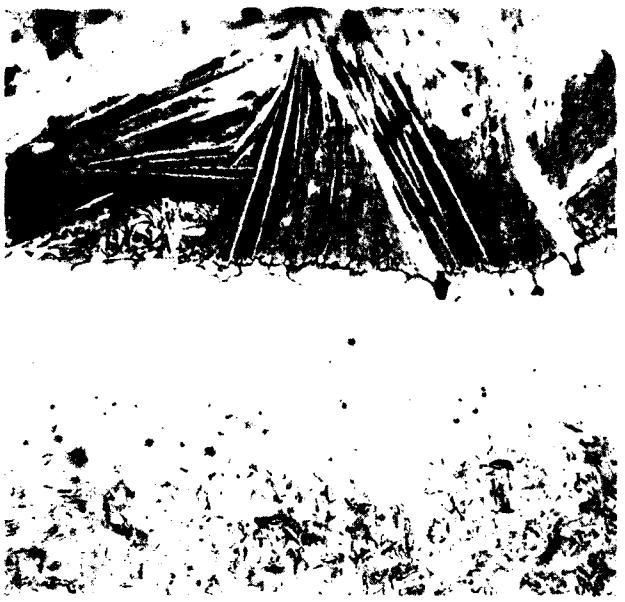

(a) 200X

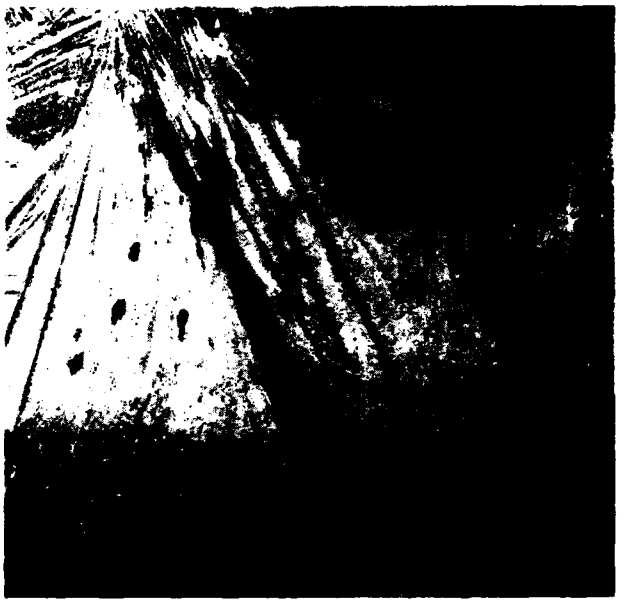

(b) 300X

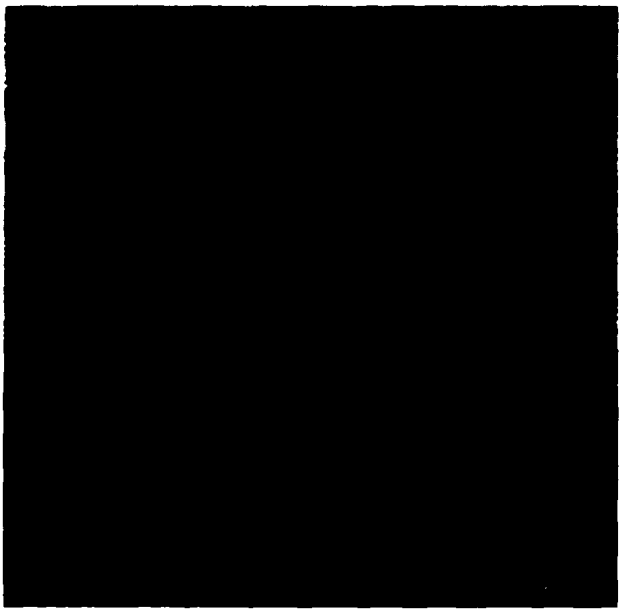

(c) 1200X

(d) 1200X

Optical (top left) and scanning electron micrographs of taper section of laboratory sample.

Figure 18

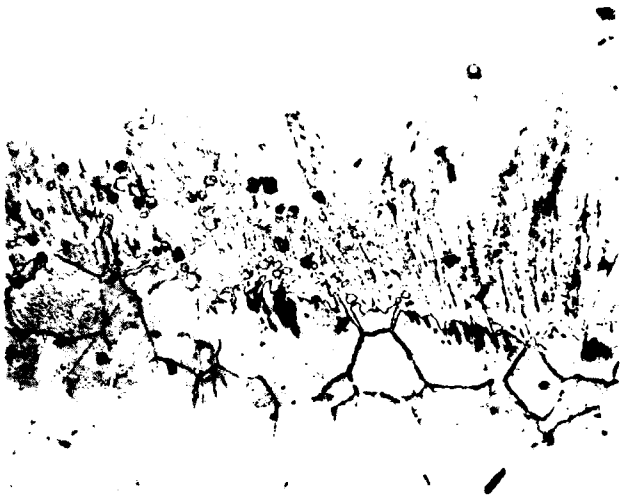

(a) 500X

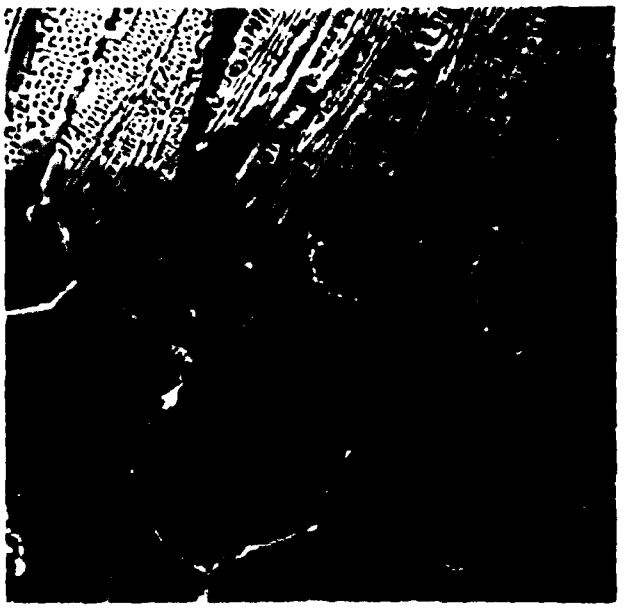

(b) 2000X

(c) 3000X

(d) 3000X

Optical (top left) and scanning electron micrographs of taper section of laboratory simulation sample.

Figure 19

(a) 3000X

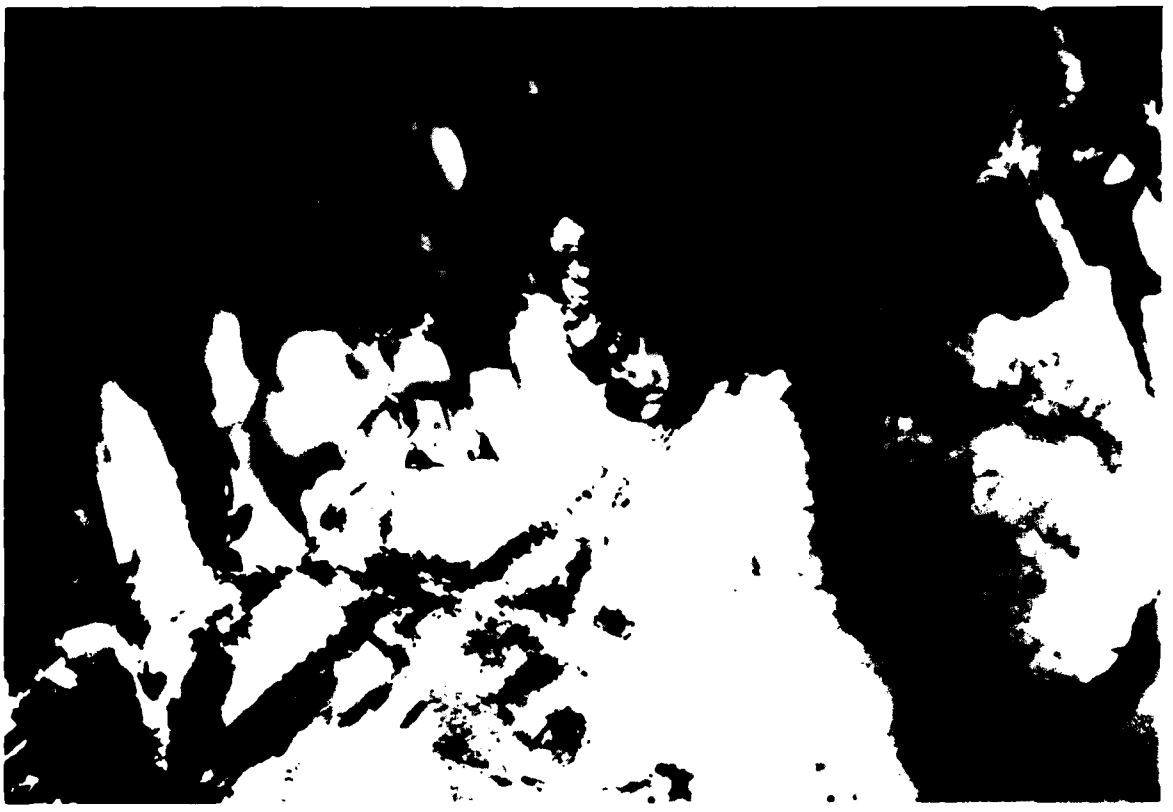

(b) 30,000X

Scanning electron micrograph and transmission electron micrograph of thin foil at carbide-austenite interface in laboratory simulation sample.

Figure 20

(a) 42,000X

(b) 30,000X

(c) 30,000X

Transmission electron micrographs of carbide-austenite interface.

Figure 21

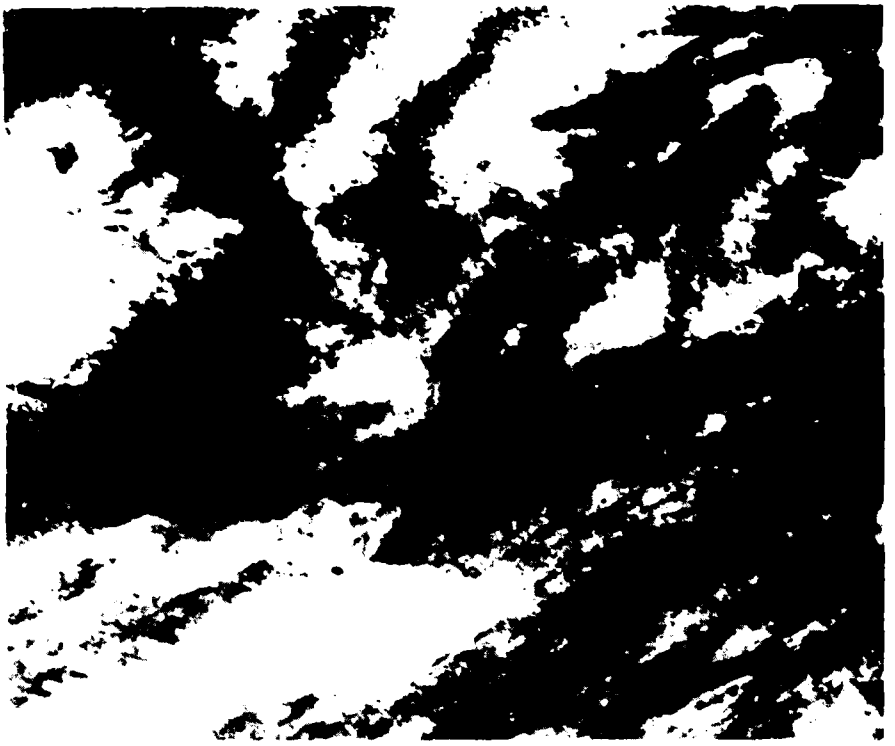

(a) 30,000X

(b) 30,000X

Transmission electron micrograph of austenite region (top) and steel matrix (bottom).

Figure 22

PART TWO

STRUCTURE OF ELECTRODEPOSITED CHROMIUM

SUMMARY

Scanning and transmission electron microscope examination of electrodeposited chromium has revealed that plating conditions affect the size and orientation of the very fine individual crystallites. Plating at 55°C results in a bright, very hard, 1180 Knoop-hardness number (KHN), coating comprised of 0.1 μm diameter grains with a strong <111> fiber texture oriented perpendicular to the surface of the base metal. Plating at higher temperatures such as 85°C, or with a well aged plating solution, produces a much softer deposit (600 KHN) composed of 1.5 μm grains with a much less pronounced crystallographic texture. High tensile stresses and the resulting crack formation in the deposit appear to be due to the very large and aligned void space associated with the unequilibrated grain boundaries. Heating during firing or annealing results in 1 or 2 percent shrinkage of the chromium as the grain-boundary void space is eliminated.

Introduction

Previous detailed studies using a variety of analytical techniques have shown that the "white layer" which forms on the bore surface of cannon barrels during firing is a consequence of intense carburization of the interior surface by the high temperature and high carburizing activity of the gas produced from the explosive charge. This results in the formation of high-carbon molten steel, which is a very corrosive medium and can cause very rapid deterioration of the interior surface, making it necessary to replace the cannon tube.

A possible means of alleviating the extent of white-layer formation is to protect the surface by applying a thin

coating, perhaps up to 100 μm in thickness, of chromium by electrodeposition. A long-standing difficulty with such thick coatings is the occurrence of extremely high tensile stresses in the plane of the deposit. These usually lead to cracking, either during the plating operation itself or during subsequent heating.

The magnitude of the tensile stresses, and the extent of the contraction that subsequently occurs, depend on the plating conditions, particularly current density and electrolyte temperature. Samples of 4340 steel, as used for cannon tubes, were electroplated with chromium at Watervliet and submitted for metallographic examination by light and electron microscopy.

The metallography of electroplated chromium is well known to be rather difficult. The grain size is generally extemely small, internal stresses are large due to high concentrations of defects, the presence of cracks can cause difficulty with polishing or thinning, and etching to reveal the microstructure is not easy because of the very etch-resistant nature of chromium.

Experimental Procedures

Four samples of chromium-plated steel, as described in Table I, were submitted for examination. One, designated as sample A, is representative of typical electroplating conditions which result in a rather hard "bright" deposit with a very high degree of contraction. Other samples electroplated under conditions which produce lower hardness and much less contraction and cracking were also submitted, along with sections of a chromium-plated cannon barrel after test firing.

Samples were mounted and polished in cross section and in planar section in order to observe the crack structures in both orientations in the light and scanning electron microscopes. The metallographic appearance of cracks in both light and electron microscopes was found to depend on preparation conditions, as

discussed in the following sections of this report.

Thin foils were prepared by ion milling for transmission microscopy in the USS million-volt electron microscope. Slices cut parallel to the surface were ground to about 50 μm in thickness. Because of the cracks, only small pieces survived this process and truly satisfactory thin foils could not be obtained in all cases.

Metallographic Observations

Optical micrographs of cross and surface sections of sample A of bright hard chromium are shown in Figure 1. No microcracks are visible on the mechanically polished surface. However, electrolytic polishing-etching does reveal the presence of numerous cracks perpendicular to the plated surface, as shown in Figure 1b, and on the planar section shown in Figure 1c. At higher magnification in the scanning electron microscope, cracks were revealed very clearly in both cross and parallel sections of the chrome plate, as shown in Figure 2. The appearance of the cracks suggested that they contain some unknown material, although this effect was not fully reproducible between the usual alternate polishing and etching cycles.

The results of very deep electroetching of the chrome plate are shown in Figure 2. It may be seen that thin films of what are presumed to be amorphous chromium oxide form at the cracks. This structure will be discussed further in a section dealing with the nature of microcracks in electrodeposited chromium.

Transmission electron micrographs of a thin foil of sample A are shown in Figure 3. The pattern of microcracks and the extremely fine grain size are illustrated at several different magnifications. The electron diffraction pattern from a selected area is also included in the figure. Indexing of the diffraction

rings reveal that the (200) reflections are completely missing. This is indicative of an extremely pronounced <111> fiber texture. The apparent grain size, as determined by dark field micrographs, as in Figure 3d, is about 0.1 μm. This grain size is about 5X larger than typical values given in the literature which were based on x-ray line-broadening measurements. The probable reason for the difference is that the grains themselves contain a very high dislocation density in a rather ill-defined substructure. The high dislocation density of about 10^{14} would markedly affect line broadening and indicate an apparent finer grain size than is actually present.

When the specimen is tilted so that <111> axes of the columnar grains are not parallel to the beam in the high-voltage microscope, a rather characteristic electron diffraction pattern appears, as illustrated in Figure 4. In this sequence of images and diffraction patterns, the foil was tilted about the axis of the crack running across the center of the field of view. The total range of tilting was 45°, that is, from $+15^{\circ}$ to -30°, as indicated on the figure. Gaps which occur in the diffraction rings and the characteristic striped pattern result from an oblique view of a fiber-textured specimen. Some micrographs of another tilt series are shown in dark field in Figure 5. One of the striking features of the microcracks is that they are discontinuous and "ligaments" of metal connect some grains all through the specimen. Presumably these connections are the reason that the foil, although extremely fragile, remains intact and can be mounted and examined in the high-voltage microscope. This crack structure will be discussed further in the following section.

The crack pattern in the electroplated chromium becomes more pronounced after heating for 1 hour at $900^{\circ}C$, and air cooling. Examples of cross and parallel sections are shown in Figure 6. It does not appear that the cracks are any more numerous than before but have become wider, presumably because of further contraction during annealing of the electrodeposit. The hardness

decreased to 160 KHN as a result of the annealing treatment. This is a larger drop than might be expected from the grain size change, indicating that part of the high hardness results from the dense dislocation substructure.

High-voltage electron micrographs after annealing sample A for 1 hour at 900°C are shown in Figure 7. These show that although recrystallization has occurred, many of the ligaments along the cracks remain. The fine structure in the matrix could be dislocation loops produced by condensation of vacancies associated with the intergranular void space. However, it is more likely that they are chromium oxides formed from the co-deposition of Cr(OH) in the grain-boundary cavities during plating.

Sample B, (chromium electrodeposited at 85°C) was examined in the manner described in the preceding section of this report. Optical micrographs of the cross and surface sections are shown in Figure 8, and scanning electron micrographs in Figure 9. It may be noted that the hardness of 650 KHN is about half that of sample A and the crack spacing is about 10X coarser. High-voltage electron microscopy of ion-thinned sections of the 85°C sample revealed a much coarser grain size and more random grain orientations, as illustrated in Figure 10.

The grain structure of the chromium in sample C, which was electrodeposited at 55°C using a used plating solution, was found to be generally similar to that observed in sample B. High-voltage electron micrographs of specimens examined as-plated and after annealing are shown in Figure 11. Annealing resulted in little grain coarsening but did produce more equiaxed grains and eliminated much of the dislocation substructure.

Scanning and high-voltage electron microscopy were also used to examine the chromium electroplate on a sample of fired cannon. Micrographs of the cross section and surface are shown in Figures 12 and 13 after mechanical polishing, and in Figure

14 after electropolishing. The grain, dislocation, and crack structures in thin foils are illustrated in the high-voltage micrographs in Figure 15. The cracks are wider and more complex after firing as compared with annealing at 870 to 900°C for laboratory samples. During firing the surface is heated to >1100°C for a few milliseconds and is also exposed to explosive pressures. More detailed study of the crack structures should be carried out.

Results and Discussion

The results of optical, scanning, and high-voltage electron microscopy of samples of chromium electrodeposited under various conditions have revealed the following salient features:

1) The grains are small, 0.1 μm in diameter, and highly oriented (<111> fiber texture) when electrodeposition occurs at 55°C. At 85°C or when old plating solution is used, the grains are much larger (1.0 to 1.5 μm) and more randomly oriented.

2) The cracking tendency decreases with increasing grain size.

3) The cracks which form along grain boundaries are discontinous and remain so after annealing.

4) The structure of the cracks is rather complex and frequently they occur as very closely spaced double cracks.

5) An amorphous film forms at the crack during electropolishing.

It appears from this study that the high tensile stresses present in electrodeposited chromium result from the fine grain

structure, and the tendency for cracking should therefore be controllable. A theoretical model for the stresses is under consideration and will be reported in due course. It suggests lower stresses in thin deposits. The cracks in sample A are spaced about 10 to 20 μm apart and are about 0.2 μm in width, which correspond to a relaxation of tensile strain of about 1 to 2 percent. Amorphous metals also shrink about 2 to 4 percent during recrystallization. The crack spacing observed here corresponds to 100 to 200 grain diameters, indicating an average void space of 10° to 20 A° per grain boundary. This amount is not unreasonable for the unequilibrated grain structure produced during electrodeposition. Although the stresses in chromium electroplate are generally found to be tensile, "compressive" stresses have been reported in some cases. Presumably such apparent compressive stress is a result of cracking during plating and the deposition of chromium (or more likely the amorphous film observed here) within the cracks during further plating.

The lower hardness obtained by plating at high temperature, or by annealing previously, results from both a decrease in dislocation density and grain coarsening. In terms of a hardness—grain-size Petch plot the contributions of these two effects are about equal. It is known that 1 to 2 percent of Cr(OH) is trapped within the deposited film, and this effect apparently results in the formation of Cr_3O_4. Some weak electron diffraction evidence for this phase was obtained in the high-voltage electron microscope.

TABLE I

Samples of Chrome Plating Examined by Electron Microscopy

Sample	Preparation	Hardness	Grain Structure
A Hard chrome Hc 12-80-1	30A/DM^2 55°C	1150 KHN (190 after annealing at 900°C)	0.1 μm Dia. strong fiber texture <111>
B L.C. chrome LC-12-80-3	120A/DM^2 85°C	650 KHN (188 after annealing at 870°C)	1.5 μm weak texture
C L.C. chrome HEX.10-80-nt	120A/DM^2 well aged bath	610 KHN	1.8 μm weak texture
D Fired cannon 8312-09-001	-	-	0.1 μm strong texture

References to Work Microstructure and Stresses of Electrodeposited Chromium

W. Hume-Rothery and M.R.J. Wyllie, Proc. Roy. Soc. (London) A181, 331 (1943); preferred orientation emphasized, covers wide range of temperature - current density for conventional bath.

C. A. Snavely and C. L. Foust, J. Electrochem. Soc. 97, 99 (1950); Cr hydride theory to account for observations about properties of Cr deposits.

H. Fry, Trans. Inst. of Metal Finishing 32, 107 (1955); microstructural study of lamination-cracking.

H. Wiegand and H. R. Kaiser, Metalloberflaeche 19, 161 (1965); virtual atlas of Cr deposit structures from sulfate and sulfate-silicofluoride catalyzed baths.

W. H. Cleghorn and J. M. West, Trans. Inst. of Metal Finishing 44, 105 (1966); stress in thin Cr, epitaxial effects.

D. R. Gabe and J. M. West, ibid 40, 197 (1963); stress and cracking.

T. E. Such and M. Partington, ibid 42, 68 (1964); stress and cracking.

D. W. Hardesty, J. Electrochem. Soc. 111, 912 (1964); interpretations of deposit and substrate stresses, possible epitaxy.

D. W. Hardesty, ibid 116, 1194 (1969); epitaxed deposits from F-catalyzed bath.

P. A. Jacquet, Compt. Rend. Acad. Sci. 256, 4209 (1963); high (optical) magnification structure of Cr.

J. K. Dennis, Trans. Inst. of Metal Finishing 43, 84 (1965); most detailed stress - thickness results.

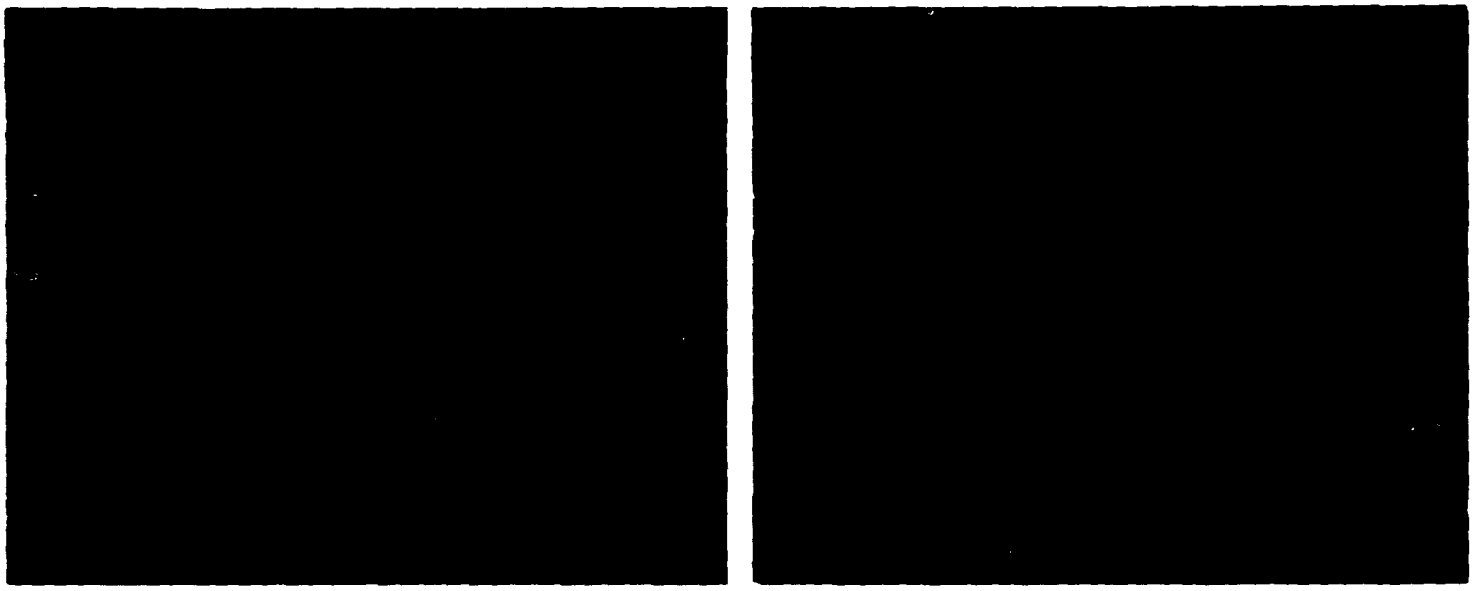

(a) 300X (b) 500X

(c) 200X

Optical micrographs of chromium electrodeposited at 55°C showing Knoop hardness values on cross section (a), and microcracks revealed by electropolishing cross section (b), and surface section (c).

Figure 1

(a) 1000X

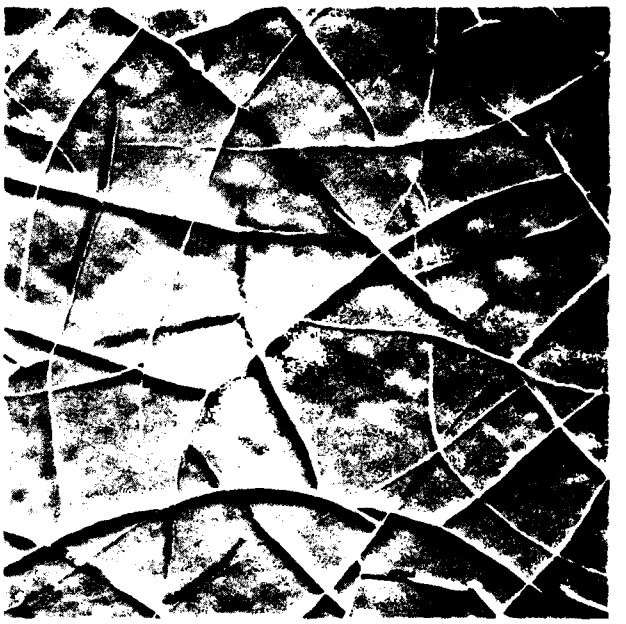

(b) 500X

(c) 200X

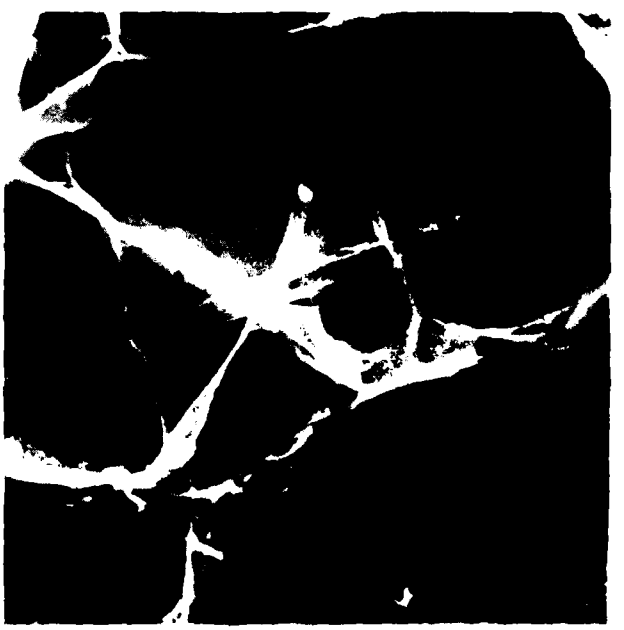

(d) 1000X

Scanning electron micrographs of chromium electrodeposited at 55°C and electropolished to reveal microcracks; cross section (a), and surface (b),(c),(d). Prolonged electropolishing enhances formation of amorphous film (c),(d).

Figure 2

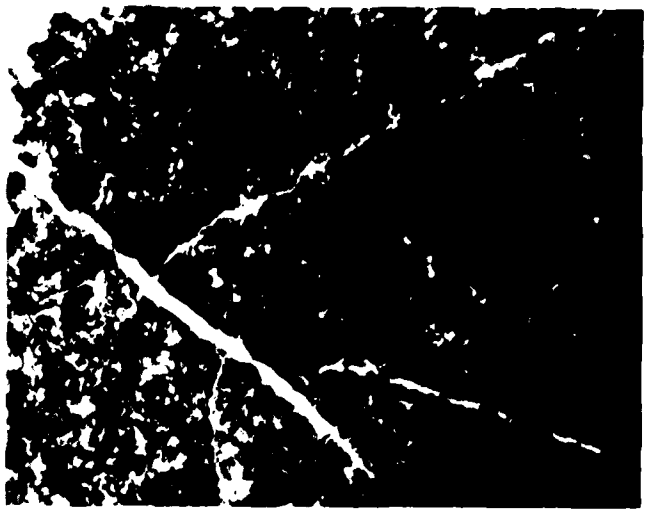

(a) 11,000X

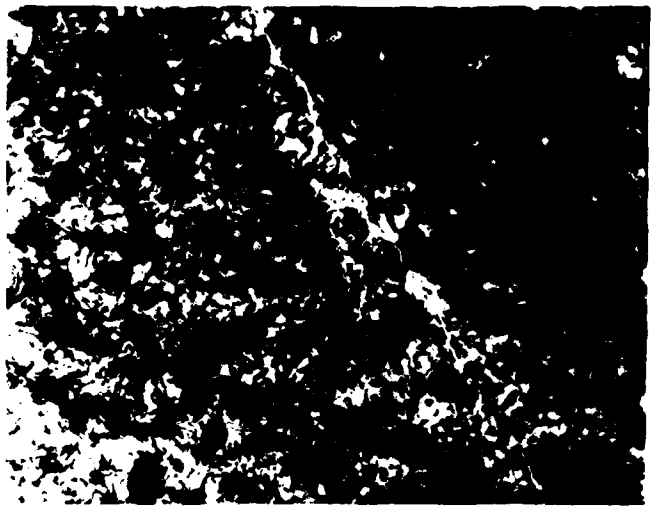

(b) 15,000X

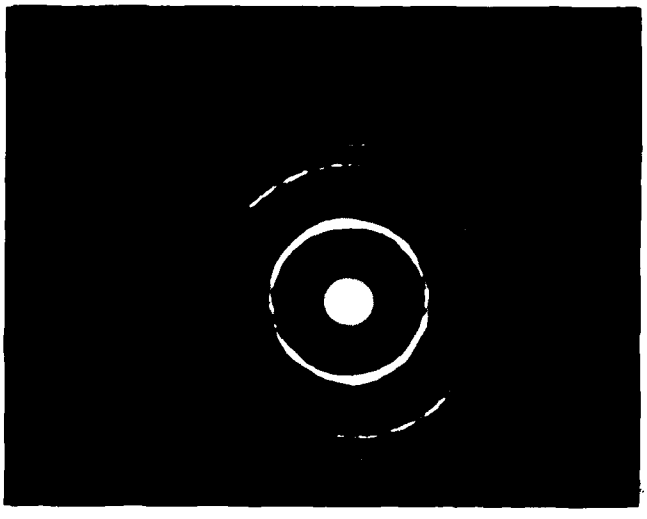

(c) SAD

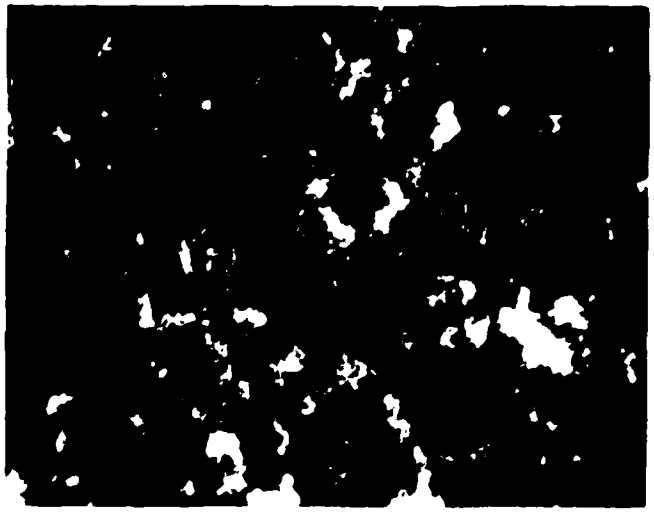

(d) 60,000X

High voltage transmission electron micrographs of chromium electrodeposited at 55°C showing microcracks (a), fine 0.1μm grain size (b), electron diffraction pattern (c), and dark field image (d).

Figure 3

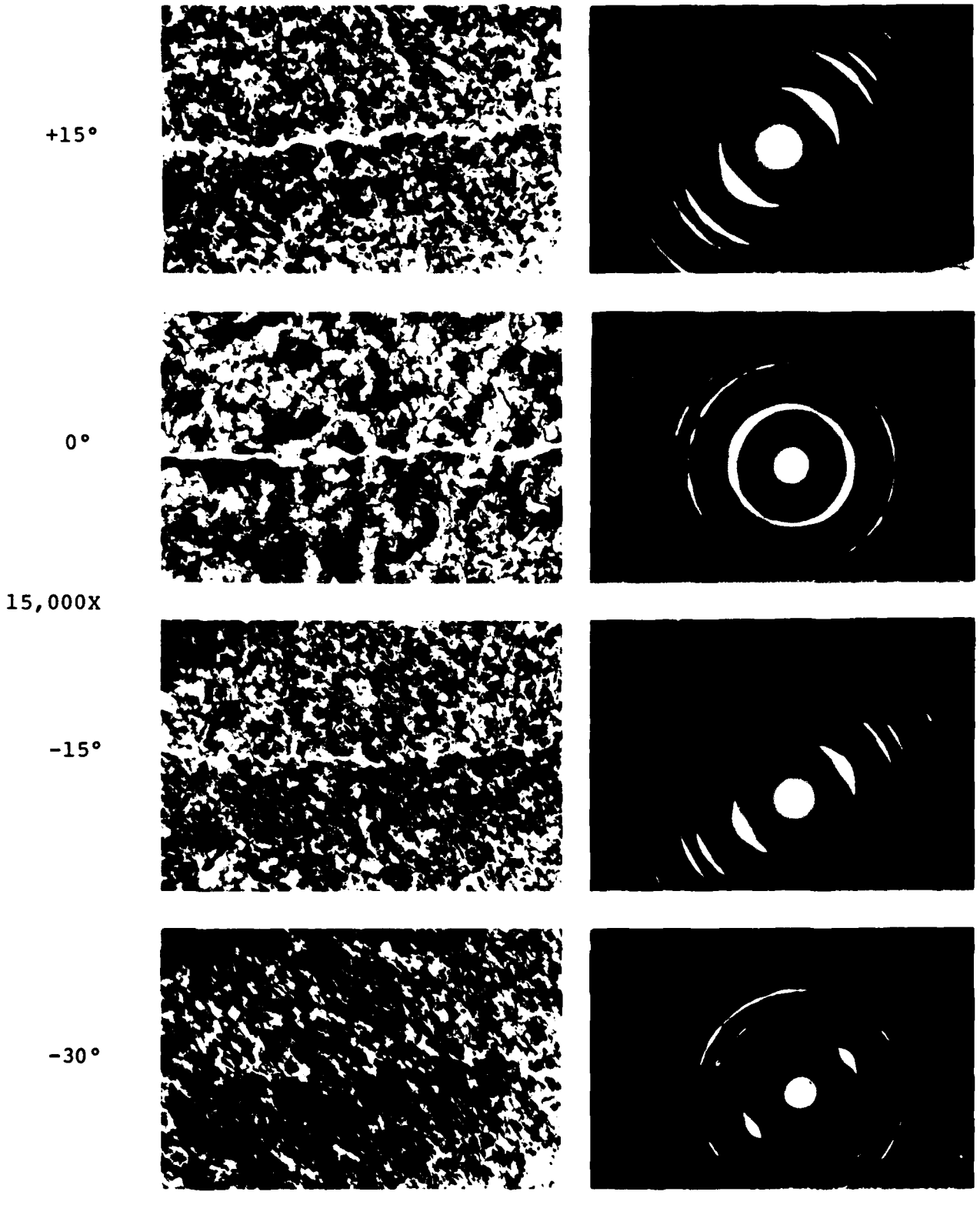

High voltage transmission electron micrographs of chromium electrodeposited at 55°C. Sample was tilted around an axis along the microcrack. Missing 200 reflection and discontinuous arcs are characteristic of a 110 fiber texture parallel to the film thickness direction.

Figure 4

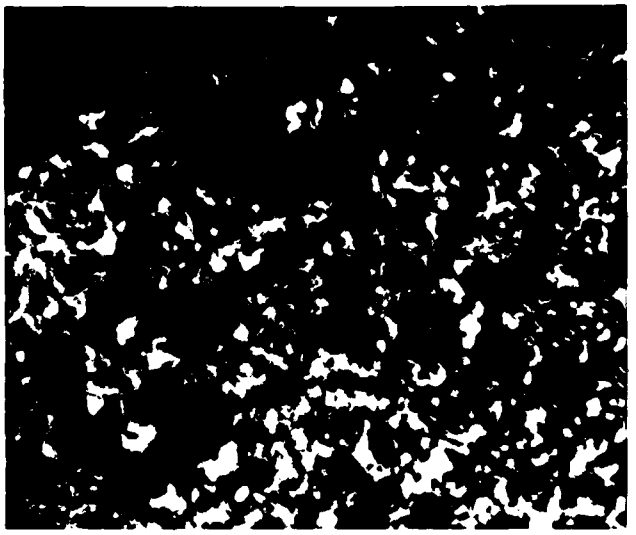

(a) +15° 15,000X

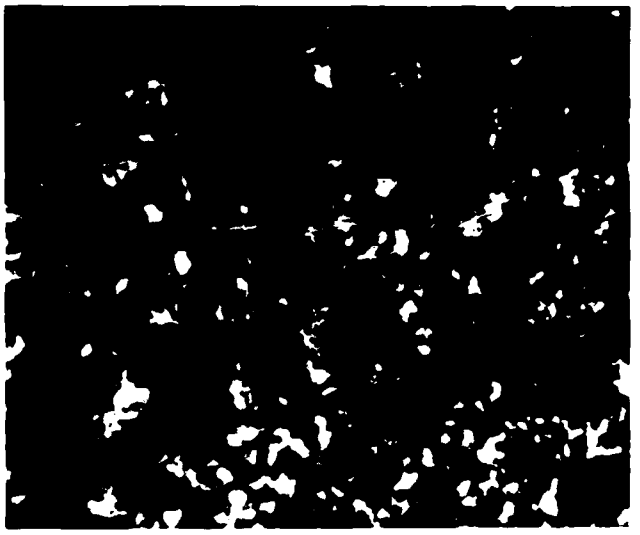

(b) 0° 15,000X

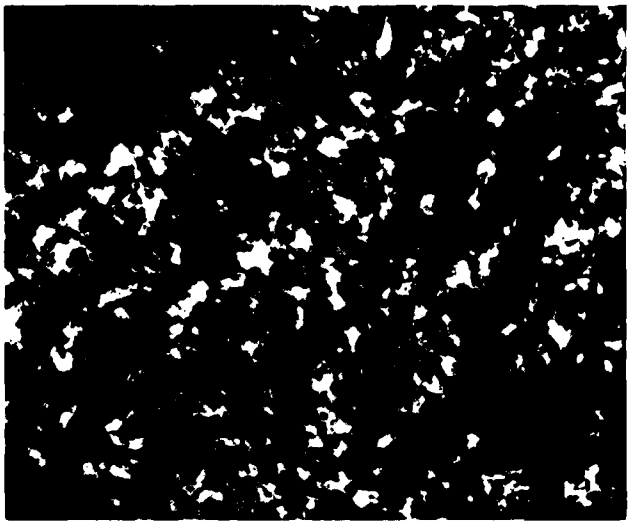

(c) -15° 15,000X

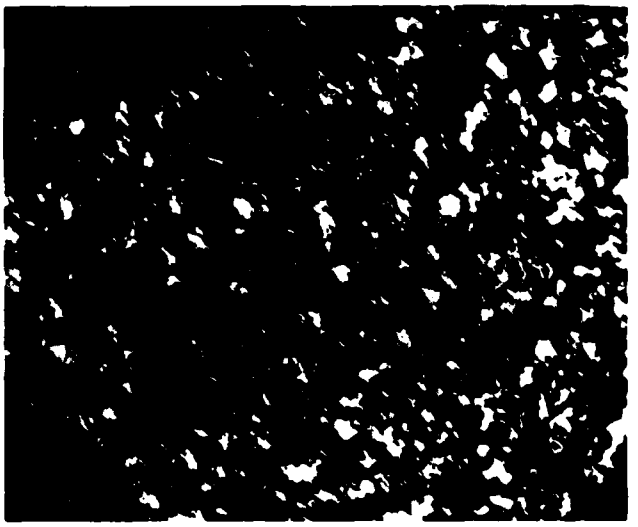

(d) -30° 15,000X

High voltage transmission electron micrographs (all dark field) showing grain clusters with similar orientations.

Figure 5

(a) 1000X

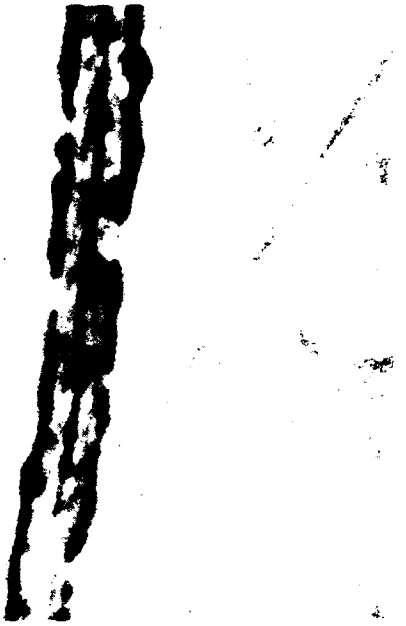

(b) 10,000X

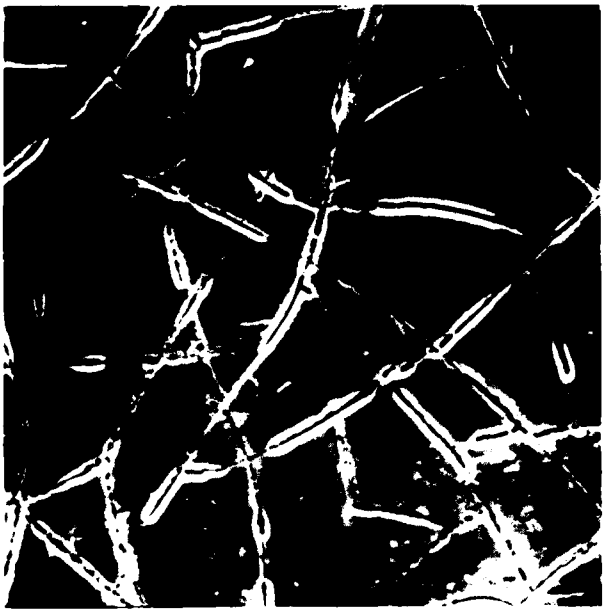

(c) 1200X

(d) 6000X

Scanning electron micrographs of chromium electrodeposited at 55°C and then annealed at 900°C for 1 hr to enlarge microcracks; both cross sections (a),(b), and surface sections (c),(d) were electropolished.

Figure 6

(a) 2000X

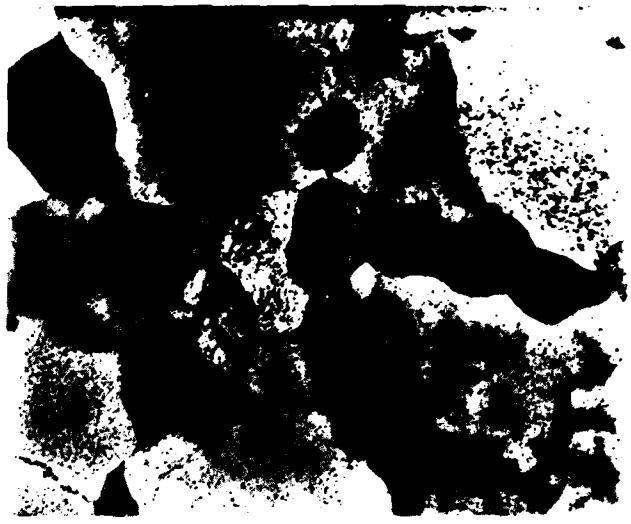

(b) 10,000X

(c) 30,000X

(d) 120,000X

HVEM transmission micrographs showing chromium electrodeposited at 55°C and then annealed for 1 hr at 900°C resulting in crack coarsening (a), recrystallization (b),(c), and formation of fine precipitates or vacancy loops (d).

Figure 7

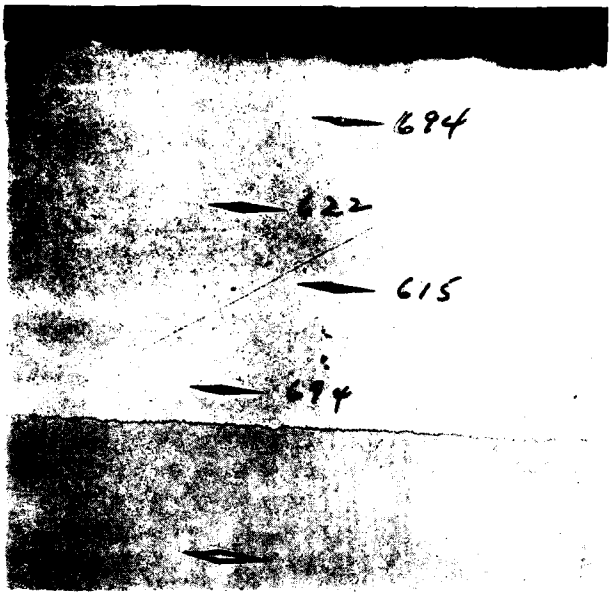

(a) 300X

(b) 500X

(c) 200X

Optical micrographs of chromium electrodeposited at 85°C showing Knoop hardness values (a), and coarse microcracks in cross section (b), and surface section(c).

Figure 8

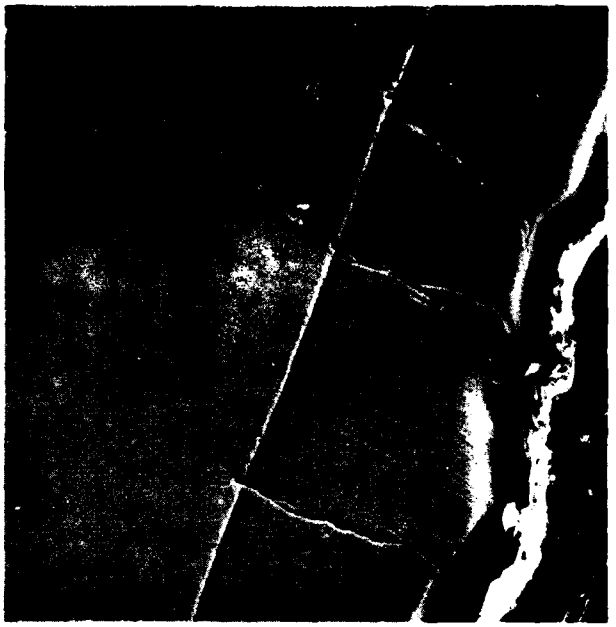

(a) 500X

(b) 5000X

(c) 100X

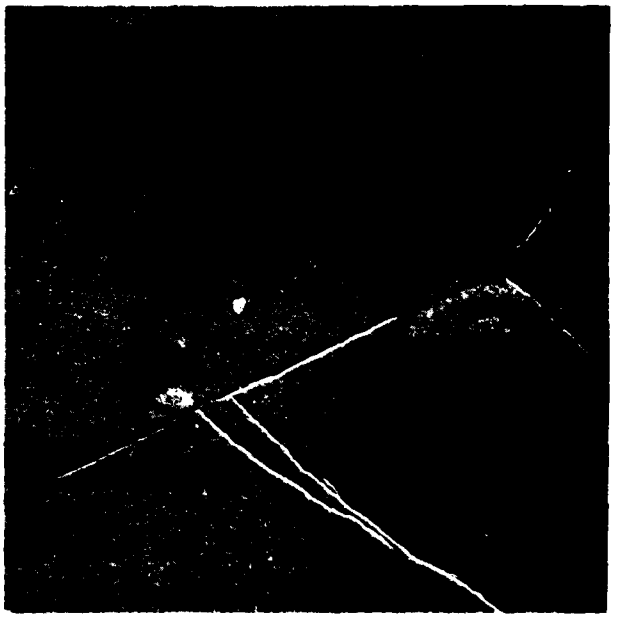

(d) 300X

Scanning electron micrographs of chromium electrodeposited at 85°C showing coarse microcrack structure; cross sections (a),(b); surface sections (c),(d).

Figure 9

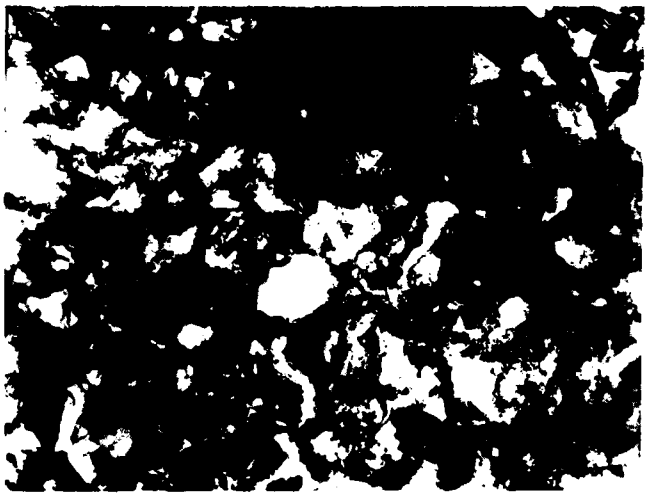

(a) 15,000X

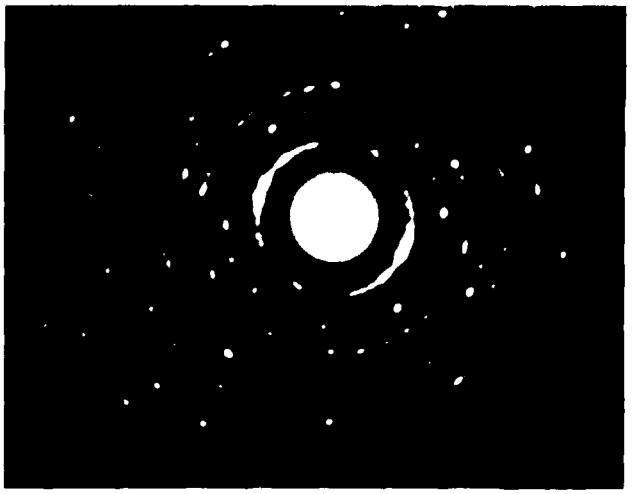

(b) SAD

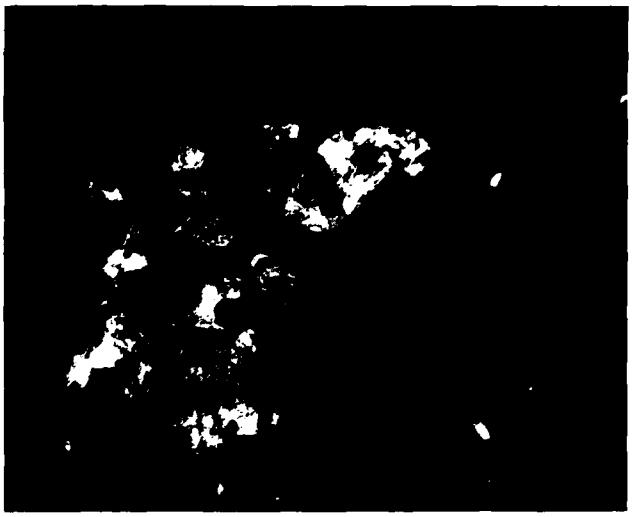

(c) Dark Field 15,000X

HVEM micrographs of chromium electrodeposited at 85°C showing dense substructure in the 1μm grains which exhibit only a weak fiber texture.

Figure 10

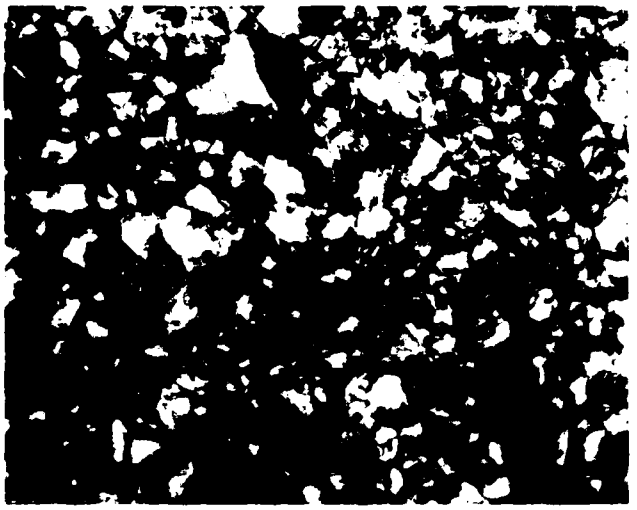

(a) 5000X

(b) 15,000X

(c) 7500X

(d) 15,000X

High voltage electron micrographs of chromium electrodeposited at 55°C with used plating solution; as deposited (a),(b), and after annealing 1 hr at 870°C (c),(d).

Figure 11

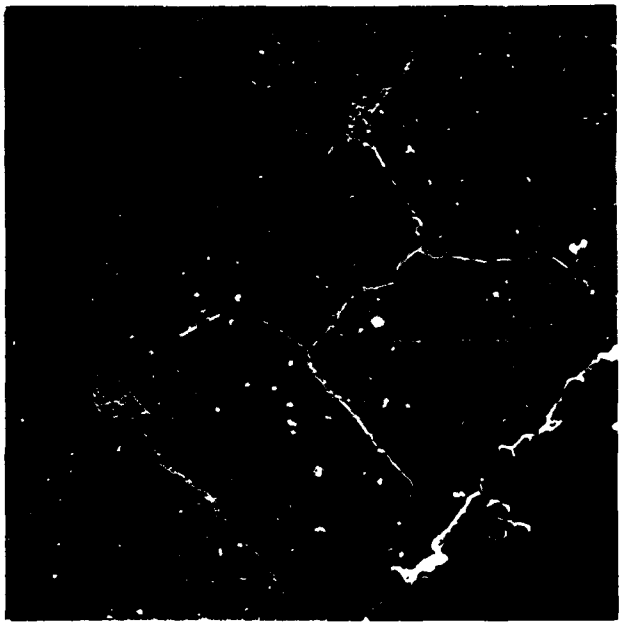

(a) 200X

(b) 500X

(c) 1000X

(d) 5000X

Scanning electron micrographs of mechanically polished cross section of chromium electroplate on a fired cannon.

Figure 12

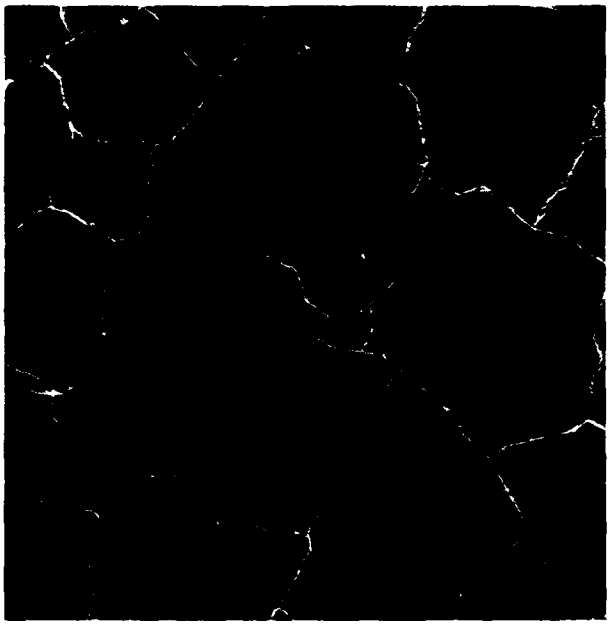

(a) 100X

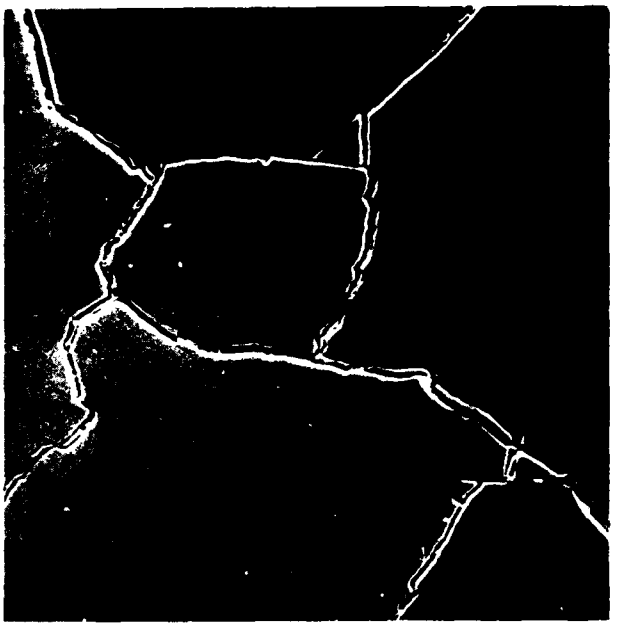

(b) 500X

(c) 1000X

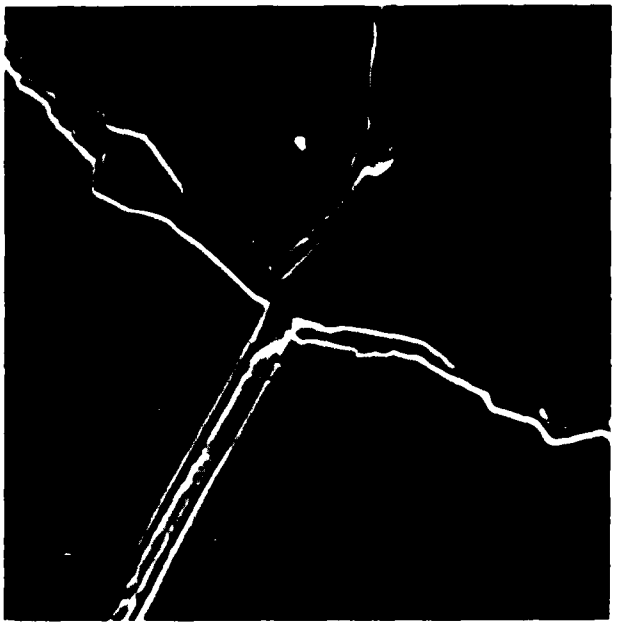

(d) 1000X

Scanning electron micrographs of mechanically polished surface of chromium on a fired cannon.

Figure 13

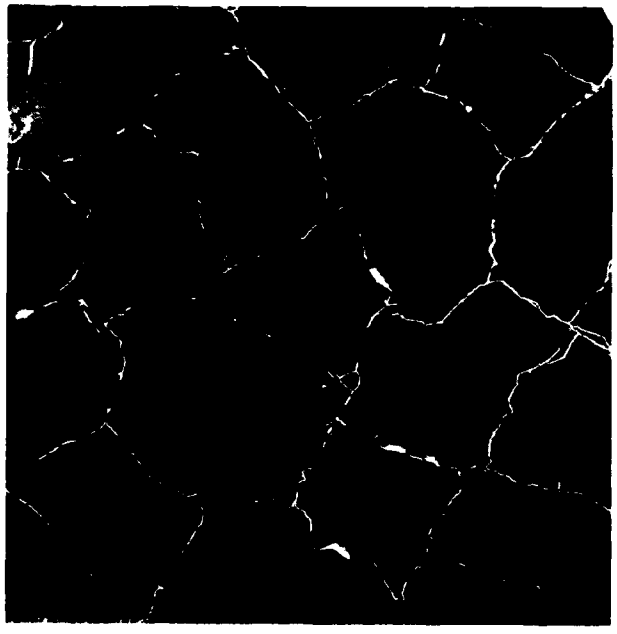

(a) 100X

(b) 200X

(c) 500X

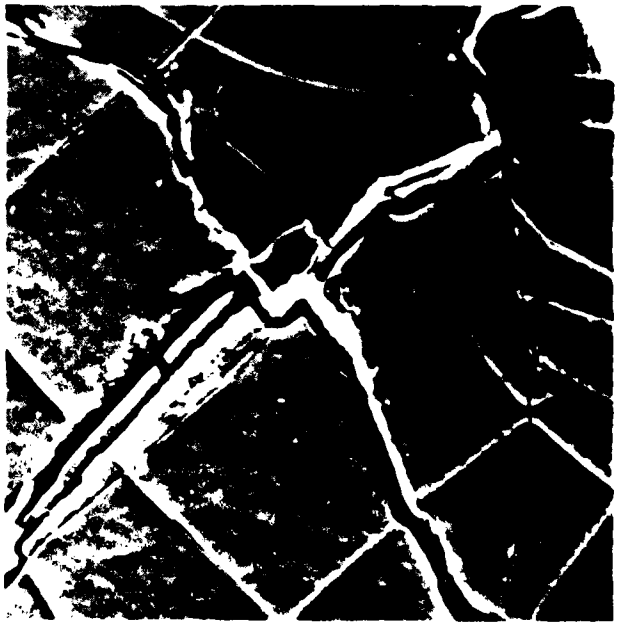

(d) 1000X

Scanning electron micrographs of electropolished surface of chromium on a fired cannon.

Figure 14

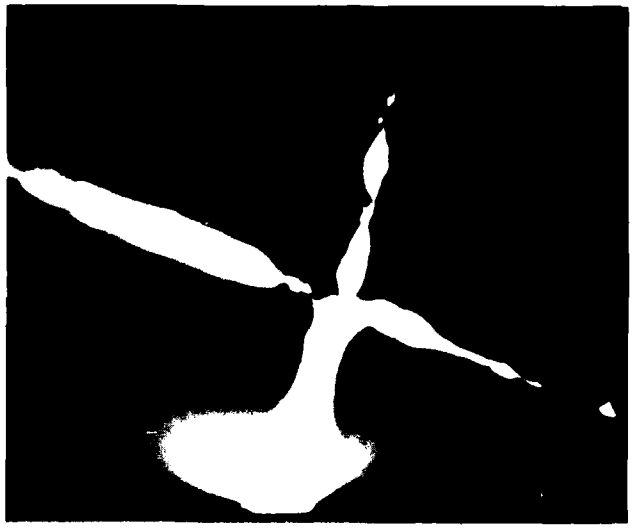

(a) 10,000X

(b) 60,000X

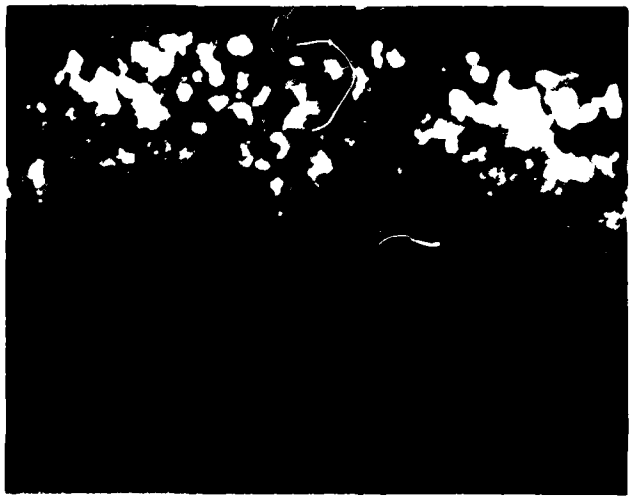

(c) 30,000X

(d) SAD

HVEM of chromium electroplate stripped from surface of fired cannon.

Figure 15

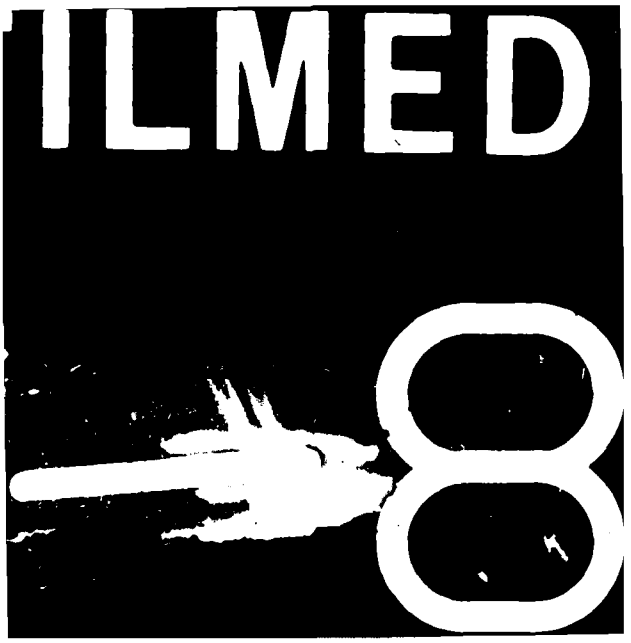
ILMED
8